[redacted]

CONFIDENTIAL

Copy 223

RM A55J28

NACA

Rq # 1.5-6 5-5

21 FEB 1956

RESEARCH MEMORANDUM

APPLICATION OF TCHEBICHEF FORM OF HARMONIC ANALYSIS TO THE CALCULATION OF ZERO-LIFT WAVE DRAG OF WING-BODY-TAIL COMBINATIONS

By George H. Holdaway and William A. Mersman

Ames Aeronautical Laboratory
Moffett Field, Calif.

NATIONAL ADVISORY COMMITTEE FOR AERONAUTICS

WASHINGTON

February 13, 1956

CONFIDENTIAL

[redacted]

G

NATIONAL ADVISORY COMMITTEE FOR AERONAUTICS

RESEARCH MEMORANDUM

APPLICATION OF TCHEBICHEF FORM OF HARMONIC ANALYSIS TO THE CALCULATION OF ZERO-LIFT WAVE DRAG OF WING-BODY-TAIL COMBINATIONS

By George H. Holdaway and William A. Mersman

SUMMARY

The techniques of the computing procedure of NACA RM A53H17 have been significantly improved by a new procedure of harmonic analysis using Tchebichef polynomials. This improved method is described in detail with illustrations of its two main advantages; these are, simplification of the computing procedures, and the provision for a comprehensive check solution which includes a direct check of how well the number of harmonics used represent the area-distribution curve. For the present, no specific recommendation can be made as to the number of harmonics which should be used for all configurations in making wave-drag computations; however, certain guides are given in the concluding remarks of the report. The new procedure is also evaluated by comparisons with analytical solutions, results from the previous method, and experimental results.

INTRODUCTION

The computing method of reference 1 has been effectively used to estimate the zero-lift drag-rise coefficients of various relatively smooth wing-body-tail combinations (refs. 2, 3, and 4). However this original method involves several operations, and the checking procedures, such as were used in reference 3, are time-consuming and check back to only the slopes of the area-distribution curves and not to the area-distribution curves themselves.

It is the purpose of this paper to present and to analyze another method for representing the slope of area-distribution curves, which will allow for a more rapid computation of wave drag and will permit the use of an improved method of checking the computations. The basic method for computing the wave drag is fundamentally the same as in reference 1 and is based on the theory of reference 5. The main difference is that

[redacted]

[redacted]

Tchebichef polynomials (refs. 6 and 7, also spelled Chebyshev) are used to represent the Fourier sine series defining the slopes of the area-distribution curves.

The new method is evaluated by comparison of results with analytical solutions, results from the previous method, and experimental results for Mach numbers up to 1.8. The configurations selected, for which experimental data were available, included models of a triangular-wing interceptor-type airplane, a swept-wing interceptor-type airplane, and a body-tail configuration with a scoop-inlet duct.

SYMBOLS

A_n	coefficients defining the magnitude of the harmonics of a Fourier sine series
C_{D_o}	zero-lift drag coefficient, $\frac{\text{drag at zero lift}}{qS_w}$
C_{D_o}'	zero-lift wave-drag coefficient, $\frac{\text{theoretical wave drag at zero lift}}{qS_w}$
ΔC_{D_o}	zero-lift drag-rise coefficient, $\frac{\text{zero-lift drag rise above subsonic level}}{qS_w}$
c	local chord measured parallel to plane of symmetry
M.A.C.	mean aerodynamic chord of the total wing
d_o	maximum body diameter
l	fuselage or body length
M	free-stream Mach number
m	duct mass-flow ratio
N	number of terms or harmonics used in the Fourier sine series
n	a harmonic of the Fourier sine series
q	free-stream dynamic pressure
S	projection of S_s on a plane perpendicular to x axis

S_s area formed by cutting configurations with planes perpendicular or oblique to the x axis

$S'(x)$ slope of S curves as a function of x, $\frac{dS}{dx}$

S_w total wing area

x distance along the x axis measured from the mid-length position

x,y,z Cartesian coordinates as conventional body axes

θ angle between the z axis and the intersection of the cutting planes X with the yz plane (See ref. 1 for descriptive sketches and detailed definitions.)

ξ distance along the x axis measured from the mid-length position divided by one half of the body length

φ transformation of the length x to radians, arc cos $\frac{2x}{l}$ or arc cos ξ

X a series of parallel cutting planes tangent to the Mach cone (At M = 1.0 these planes are perpendicular to the x axis.)

ψ angle in the xy plane forward between the y axis intercept of the cutting planes X on the xy plane, arc tan $(\sqrt{M^2-1} \cos \theta)$

$T_n(\xi) = \cos n\theta$ Tchebichef polynomial, reference 6

$V_n(\xi) = \frac{\sin n\theta}{\sin \theta} = U_{n-1}(\xi)$ Tchebichef polynomial, reference 6

COMPUTING METHOD

A summary of the computing method is presented here, with the complete details given in the appendix. As shown in reference 1 (based on the theory of ref. 5), the wave-drag equation may be written in coefficient form as

$$C_{D_o}' = \frac{1}{\pi S_w} \int_0^{2\pi} \sum_{n=1}^{\infty} n A_n^2 d\theta \qquad (1)$$

where A_n is considered as having a length dimension and is defined as

$$A_n = \frac{2}{\pi} \int_0^{\pi} S'(x) \sin n\varphi \, d\varphi \tag{2}$$

Introduce the variable, $\xi = \frac{2x}{l} = \cos \varphi$; then equation (2) may be written,

$$A_n = \frac{4}{\pi l} \int_{-1}^{1} S'(\xi) \frac{\sin n\varphi}{\sin \varphi} \, d\xi \tag{3}$$

where the limits are defined in figure 1:

$$-\frac{l}{2} \leq x \leq \frac{l}{2}$$

$$-1 \leq \xi \leq 1$$

$$\pi \geq \varphi \geq 0$$

Introduce the Tchebichef polynomial, reference 6:

$$V_n(\xi) = \frac{\sin n\varphi}{\sin \varphi}$$

Then equation (3) for the coefficients of the Fourier sine series may be written such that the integrand is a function of one variable:

$$A_n = \frac{4}{\pi l} \int_{-1}^{1} S'(\xi) V_n(\xi) d\xi, \qquad n=1,2,3, \ldots \tag{4}$$

Because of this simplification the computation of these coefficients and the summation $\sum_{n=1}^{N} nA_n^2$ can be performed by one continuous operation on a digital computing machine. Likewise, a reverse check computation can be performed by one machine operation. The wave-drag coefficients are computed from equation (1) by a simple integration as was done in reference 1.

There are definite advantages which are characteristic of the new computing method. It eliminates the intermediate steps of the previous method (ref. 1) consisting of computing the slopes $S'(x)$, plotting $S'(x)$ as a function of φ, and then reading this slope curve. The new method works directly from the area-distribution curves of the model. An additional machine operation has been programmed (see the appendix) which permits a check computation from the A_n coefficients back to the area curve. This is an all-inclusive check which may also be used to evaluate

the adequacy of the selected number of harmonics used in representing a particular curve. Supervision of the computation is cut to a minimum by the previously mentioned improvements.

The machine time required to make computations by the new method is one-half that of the previous method (ref. 1). This comparison does not include the time lost using the previous method due to data handling between steps. The time required to determine the area distribution of the models is not considered in this report and would not vary between the wave-drag computation methods. To compute the Fourier sine series solutions (25 harmonics) from punched data cards representing one area curve, using a Magnetic Drum Calculator, only 5 minutes are required. The check solution requires about 10 minutes. Thus on the assumption that five area curves are required per Mach number computation, the machine time required for the Fourier solution using the improved method would be less than 1/2 hour; and the checking time, less than 1 hour.

A complete derivation of the new computing method and the checking procedure are given in the appendix which contains:

1. Transformation to Tchebichef form for computing Fourier coefficients
2. General integration procedure
3. Tchebichef integration coefficients
   (a) Linear approximation
   (b) Quadratic approximation
4. Checking procedure
5. Construction and checking of tables (available on punched data cards upon request)
6. Theory and Properties of Tchebichef Polynomials

RESULTS AND DISCUSSION

An evaluation of the new computing method will be discussed in three parts: known analytical solutions compared with computed values of the Fourier coefficients; previous solutions from reference 3 compared with new computed values of the drag parameter $\sum_{n=1}^{N} nA_n^2$; and available experimental values of drag-rise coefficients compared with computed values of wave-drag coefficients at zero lift.

Check of Method by Analytical Solutions

The first known solution considered will be that for a Sears-Haack body. The shape of this minimum-drag body for prescribed volume and length is defined in figure 2. The fineness ratio of 12.5 and the actual dimensions were arbitrarily selected. The theoretical equation for the zero-lift wave-drag coefficient (C_{D_o}', fig. 2) is seen to be independent of Mach number (for slender bodies or for Mach numbers near 1.0). Also note that the derivative of the area curve is exactly equal to $A_2 \sin 2\varphi$ where A_2 defines the magnitude of the $\sin 2\varphi$ curve. The coefficient A_2 is the only nonzero term; therefore equation (1) simplifies to

$$C_{D_o}' = \frac{\pi}{2S_w} A_2^2 \tag{5}$$

where, in this case, the reference area (S_w) is replaced by the body maximum cross-sectional area for a body-alone test; that is,

$$C_{D_o}' = \frac{2A_2^2}{d_o^2} = \frac{9}{8} \pi^2 \left(\frac{d_o}{l}\right)^2 \tag{6}$$

and

$$\sum_{n=1}^{\infty} nA_n^2 = 2A_2^2 = \frac{9}{8} \pi^2 \left(\frac{d_o}{l}\right)^2 d_o^2 = 206.521 \text{ sq in.}$$

For the dimensions selected, $d_o = 53.9198$ inches.

For comparison with this theoretical solution, the area curve in figure 2 was analyzed by the new method using Tchebichef polynomials. The areas were computed for 200 equal increments of x, data cards were punched, and the A_n values were computed for 25 harmonics with the results as shown in table I. Even for the linear approximation (see appendix) between data points of $S(\xi)$, the value of $2A_2^2$ equal to 206.502 is in excellent agreement with the theoretical value of 206.521, and the total summation $\sum_{n=1}^{25} nA_n^2$ equal to 206.731 shows an error only on the order of 1/10 of 1 percent. For all harmonics other than the second the coefficients should be zero. The areas from the check solution agreed well with the original values for this case, with errors less than the possible errors in the original data (0.05 percent of $S(\xi)$ maximum). For a body that is closed at both ends the first coefficient of the Fourier sine series is always equal to zero, as in the solution presented in table I. For a body which does not close at the ends, the first term $1A_1^2$ represents the function of wave drag for a von Kármán ogive on an infinite cylinder.

The cylinder cross-sectional area is equal to the base area of the body or is equal to the base area minus inlet area in the case of a ducted model.

The second known solution considered will be that for a simplified area curve with a discontinuity of slope. This curve was selected in order to check the over-all computing procedure for all values of n from 1 to 25, because the previous Sears-Haack case primarily checked the computation of the second harmonic. The area curve is shown by the small insert in figure 3(a) and is defined:

$$S(\xi) = 0 \text{ for } -0.6 < \xi < 1.0$$

and

$$S(\xi) = -(\xi + 0.6) \text{ for } -1.0 < \xi < 0.6$$

The coefficients A_n were computed by hand from the relationship

$$A_n = -\frac{4}{\pi l n} T_n \Bigg]_{-1.0}^{-0.6}$$

These hand-computed values of A_n are compared with machine computations based on the area curve read at 200 equal intervals (table II). Note that the machine solutions agreed very well with the hand computed values (within five decimal places). These machine-computed values of A_n were used to compute the check solutions shown for both the area curve (fig. 3(a)) and the derivative of the area curve (fig. 3(b)). The area curve is enlarged in the region of the discontinuity of interest ($\xi = -0.6$) in order to show the check solution differences (fig. 3(a)). At this discontinuity the maximum error is 2.3 percent of $S(\xi)$ maximum, otherwise the error is less than 1 percent. This type of check solution gives an obvious geometric picture of the accuracy of the computation for the number of harmonics used relative to the accuracy with which the original area curve is computed.

Although not required by the new computing method, the derivative of the entire area curve is shown as the solid line in figure 3(b). This slope curve is plotted against φ in the manner used in the previous method of computing wave drag (ref. 1). The circular check points were computed by the method of reference 3, but the same values of A_n (based on Tchebichef polynomials, fig. 3(a)) were used. The overshoot of the check points near the discontinuities is due to the Gibbs phenomenon (ref. 8) and is not truly an indication of the accuracy of the Fourier coefficients, A_n. The interpretation of this type of check solution, relative to errors in area, is not obvious and is certainly more difficult than the check of figure 3(a). This difficulty was also apparent for some of the check cases presented in reference 3.

[redacted]

Check of Method by Prior Solutions

Although more involved, the previous computing method has been fairly successful in evaluating wave drag; therefore, a direct comparison between the two methods of the solutions of the drag parameter $\sum_{n=1}^{N} nA_n^2$ was made.

From reference 3, two area curves were selected which had similar total summations $\sum_{n=1}^{24} nA_n^2$, one curve having a discontinuity in slope of the area curve (figs. 4(a) and 4(b)). The drag parameters $\sum_{n=1}^{N} nA_n^2$ computed by the two methods are compared in table III. The agreement indicates that the Tchebichef solutions are comparable within 2 to 3 percent even for a curve with a discontinuity of slope. Due to the reduced number of operations involved, the new method has less chance for error.

The check solutions, of these two area curves shown in figure 4, were computed by the new method, using the Tchebichef values of A_n (table III). As was noted in reference 3, the check solutions indicate a fairly satisfactory fit of the area curve in the case of figure 4(a), and an incomplete solution for $N = 25$ in the case of figure 4(b). However, in contrast with the check solutions of reference 3, these check solutions directly show the errors in area.

Check of Method by Experimental Results

Available geometric and experimental data for three models were utilized to check the new method: a triangular-wing interceptor-type airplane model, a swept-wing interceptor-type model, and a free-flight model having tail surfaces but no wing (this model was also considered with a large scoop-inlet and duct system).

Triangular-wing interceptor-type airplane model - Model 1.- The dimensions and pertinent geometric data of the model are presented in figure 5 (data from ref. 9). The experimental data, also from reference 9, are shown in figure 6 with the computed results and model cross-sectional area distribution. The experimental drag coefficients are identified as minimum-drag coefficients, because the lift varied from approximately zero lift at low subsonic and high supersonic speeds to a peak value of $C_L = 0.05$ at $M = 0.97$. The friction-drag coefficients were approximated by the method used in reference 10. The empirical correction factor of

1.15 suggested (ref. 10) for the body portion was not applied since good agreement was obtained with the subsonic drag coefficients without such correction.

The agreement between the experimental and theoretical total-drag-coefficient curves (fig. 6) is considered to be good, with errors less than 10 percent of the experimental minimum-drag coefficients. The error in percentage of the wave-drag-coefficient increment, assuming the friction-drag variation is correct, would be increased to almost 16 percent. An assumption of no variation in friction-drag coefficient with Mach number would indicate essentially no error at all supersonic speeds. As was discussed in reference 3, the theory does not apply when the leading edge of a wing with a rounded leading edge becomes sonic. For this configuration the leading edges of the horizontal stabilizers are supersonic for Mach numbers greater than approximately 1.4 and the wing leading edge is supersonic for Mach numbers greater than approximately 1.6. Inasmuch as the wing is thin and the horizontal tail is a small part of the total configuration, the computations at $M = 1.8$ are considered to be a fair approximation in spite of the violation of the assumptions of the basic theory. The leading edge of the vertical surface of the tail is not sonic until $M = 2.0$.

As a secondary evaluation of the computations for this triangular-wing model, area curves with check solutions ($N = 25$) are presented in figure 7 for Mach numbers of 1.0, 1.2, and 1.8. These curves illustrate the degree of error in the area curves which are apparently tolerable, in view of the good computed drag-coefficient results shown in figure 6. This suggests that the area curves are effectively smoothed by boundary-layer or separation effects. For the $M = 1.0$ curve (fig. 7(a)), computing additional terms of the series would probably improve the agreement between the check curve and the original curve, but would increase the disagreement with the drag-rise coefficients at $M = 1.0$. The check solutions for the $M = 1.2$ curves (figs. 7(b), 7(c), and 7(d)) are considered to be satisfactory because only slight radii changes to the original body would be required to give areas which would match the check curve. Experimental results have indicated that small changes in area of this order or less would have little effect on the wave drag. The check solutions for the $M = 1.8$ curves (figs. 7(e) and 7(g)) are considered on the basis of the area curves alone to be questionable, particularly for the 270° cut (fig. 7(g)).

In this case, for the $M = 1.8$ computations, additional harmonics over the 25 used are evidently required to improve the agreement between the area curves. Increasing the harmonics to 49 gave agreement between the area curves and the check solutions (generally within the width of the line), with the maximum error (270° cut) being less than 2-1/2 percent of the local area curve values. The computed wave-drag coefficients for $N = 49$ were 8 percent greater than the experimental drag-rise coefficients at $M = 1.8$ (fig. 6). Increasing the number of harmonics above 49 would

further improve the agreement with the area curve, but would increase the disagreement with the experimental drag results. This tends to support the previously mentioned fact that at $M = 1.8$, the supersonic leading edges of the blunt airfoil sections are in violation of the theoretical limitations of smoothness or slenderness.

Swept-wing interceptor-type airplane model - Model 2.- The dimensions and pertinent geometric data of this model are presented in figure 8. The dimensions shown were taken from layout drawings furnished by the manufacturer for this particular version. The layout drawings also contained details as to fillets, etc., from which comprehensive area distributions were computed. Flight-test results were obtained from reference 11 for a model of a similar low-tail version of the airplane. The area distributions for Model 2 and the model of reference 11 are compared in figure 9. The essential difference between the models is that the low-tail version of reference 11 had thinner tail surfaces. In addition the fuselage lines on the model of reference 11 were faired to a point ahead of the proposed nose-inlet location and the model had no duct.

The two area curves shown in figure 9 were analyzed by the new computing method ($N = 25$) which gave wave-drag coefficients for $M = 1.0$. The computed results are compared in figure 10 with experimental drag-rise coefficients from reference 11. The only exact comparison which can be made is for the experiment and computation for the model of reference 11 for $M = 1.0$. The perfect agreement is fortuitous, particularly at a Mach number of 1.0, but still this is a favorable indication for the new computing method. The difference between the computed results for the two models ($M = 1.0$) is only slightly over 10 percent, based on the experimental results.

The computations at the two higher Mach numbers had to be made for the airplane for which detailed area distributions were available; therefore, a direct comparison between the theory and the experiment cannot be made. However, the differences at these higher Mach numbers should be of the order of the differences at $M = 1.0$ (or less), thus reasonable agreement is indicated. No correction for friction drag was made in this case; however, the prior example showed that the variation in friction-drag coefficient with Mach number would be slight. Computations were not attempted above $M = 1.4$ because sonic leading edges of the fairly thick wings with rounded leading edges would produce abrupt changes in area distribution which definitely exceed the theoretical limitations. For this type of wing the 25-term solution does not closely fit the original area curve in the region of the discontinuity, as shown in reference 3 and figure 4(b).

Scoop-inlet-duct model - Model 3.- The results of the experimental investigation of this model have not been published; however, the test procedures were identical with those of reference 12. Details of the models and a brief discussion of the experimental data accuracy are included, so that comparisons with wave-drag coefficients computed by the new method may be correctly evaluated. The dimensions of the basic body

and the ducted version are given in figure 11 and tables IV and V. The tests of the scoop-duct version were made at duct mass-flow ratios of approximately 0.6 and 0.9 using two duct nozzles with different throat sizes. The accuracy of the instrumentation and the accuracy of the final data were similar to the values of reference 12. For the scoop model, particularly for the test with a mass-flow ratio of 0.6, the errors at subsonic speeds were increased, due to fluctuation of duct pressures, to a possible maximum error in drag coefficients of ±0.02.

The experimental results for Model 3 are presented in figure 12. The internal drag coefficients (computed by the method used in ref. 12) were subtracted from the total drag coefficients at each data point to obtain the external drag coefficients. External drag-rise coefficients were measured relative to the experimental data at a Mach number of 0.8 (fig. 12(b)). The small differences between the experimental drag-rise coefficients at the two different mass-flow ratios are probably not significant in view of the possible errors in these data at subsonic speeds. The external drag-rise coefficients of the basic model are of course more accurate than for the ducted models, because the basic data were more accurate and no correction for internal drag was required.

Computed wave-drag coefficients are also shown in figure 12(b). The computation for the basic model was straightforward, checks were satisfactory, and the agreement with experimentation can be considered as another check of the new method of computation (differences ≈ 10 percent or less). In the computations for a mass-flow ratio of 1.0 it was assumed that a streamtube equal to the duct-inlet area passed through the duct relatively undisturbed without contributing to the external drag coefficients (fig. 13). The duct-inlet area was removed as a constant value from fuselage station 81.5 (duct inlet)to station 134 (duct exit). The area difference between the duct inlet and the exit was added as a constant value to the ordinates of the portion of the model aft of the duct exit, on the assumption that the increased diameter of the streamtube is maintained and affects somewhat the external wave drag. Another simplified procedure for determining the equivalent area distribution was tried which, in this case, gave essentially the same results. The area removed was determined by taking a straight-line variation from the inlet area to the exit area. As in the prior method, this procedure removed the steps (at the inlet and exit) in the original area curve.

The computed wave-drag coefficients for $(m_1/m_0) = 1.0$ were compared with experimental drag-rise coefficients for $(m_1/m_0) \approx 0.9$, inasmuch as the experimental variation of external drag-rise coefficients with mass-flow ratio is slight at transonic speeds (e.g., see data of ref. 13, converted to drag-rise coefficients). Agreement between experimental and computed values is good with maximum differences of the order of 6 percent of the experimental values. This example is not considered as a firm indication of the accuracy of the computing method because the experimental data could be in error by 10 percent. Within the evident accuracy of the

theory and experiment, the check solution for N = 25 (fig. 13) indicates an adequate representation of the area curve. Additional terms would be required for an exact fit.

The computations for a mass-flow ratio of 0.6 used the latter described procedure for removing area. Removing an area varying linearly from 0.6 of the inlet area to 0.6 of the exit area left sizable steps in the area curve (solid line, fig. 14). These large steps in the area curve result in infinite slopes and a configuration which is outside the intended limits of the theory. Some arbitrary fairings could be inserted at the duct inlet based upon estimated location of the shock wave ahead of the duct, but even this fairing would be rather abrupt and would not remove the discontinuity at the exit. Additional theory and experimentation are required to know how to correctly handle this type of discontinuity. In spite of these limitations, a 25-term computation was made to clarify the difficulties and to illustrate why the computation is an inadmissible one. The computed wave-drag coefficients for a mass-flow ratio of 0.6 predict a large increase in drag-rise coefficient with a decrease in mass-flow ratio from 1.0 to 0.6. However, as in reference 13, the experiments indicate little variation in drag-rise coefficient with mass-flow ratio.

The check solutions for N = 10 and N = 25 (fig. 14(a)) indicate that the 25-term solution is not adequate to fit the curve and at least double the number of terms would be required to even approach a close fit. Increasing the number of terms above 25 would of course increase the disagreement with measured drag coefficients, and this case is clearly an inadmissible computation.[1] At present it is recommended, for ducted configurations, to make the computations of wave drag only for a mass-flow ratio of 1.0, and estimate the possible variations with mass-flow ratio from experimental results.

CONCLUDING REMARKS

The use of Tchebichef polynomials simplifies the computation of zero-lift wave drag and provides a direct check of how well the number of harmonics used represents the area-distribution curve. For relatively smooth distributions of area, about 25 harmonics are usually sufficient to represent the area curve and to compute wave drag in reasonable agreement with experimental data.

Even for complex airplane configurations with slight discontinuities in slope of the area distribution, 25 harmonics gave reasonable agreement

[1]It was of interest to note that a very arbitrary selection of 18 terms gave drag results in agreement with the experimental data, but the check solution for 18 terms (fig. 14(b)) resulted in an extreme fairing of the area curve.

with the measured drag rise although the calculated values were for a smoothed area distribution. This suggested that small discontinuities might actually be smoothed by boundary-layer or separation effects.

On the other hand, for configurations with large discontinuities in slope (e.g., produced by a duct with a mass-flow ratio other than 1.0), the computed "smoothed" area distribution and wave drag varied markedly with the number of harmonics. This is to be expected because if an infinite number of harmonics were used, an infinite drag would be predicted when there is a step in the area curve.

In contrast a smooth body may require very few harmonics (as low as 1 or 2) to give an exact fit of the area curve and an accurate wave-drag prediction.

Ames Aeronautical Laboratory
National Advisory Committee for Aeronautics
Moffett Field, Calif., Oct. 28, 1955

APPENDIX A

TCHEBICHEF FORM OF HARMONIC ANALYSIS

Transformation to Tchebichef Form for Computing Fourier Coefficients

In reference 5 the streamwise variation of cross-sectional area $S(x)$ is expanded in a Fourier sine series in φ:

$$\frac{dS}{dx} = \sum_{n=1}^{\infty} A_n \sin n\varphi, \qquad -\frac{l}{2} \le x \le \frac{l}{2} \tag{A1}$$

where the Glauert angle, φ, is given by

$$\cos \varphi = \frac{x}{l/2}, \qquad 0 \le \varphi \le \pi \tag{A2}$$

The basic problem then is to devise a practical procedure for computing the Fourier coefficients, A_n. To begin, they are given by the classical formula of harmonic analyses:

$$A_n = \frac{2}{\pi}\int_0^{\pi} \frac{dS}{dx} \sin n\varphi \, d\varphi \tag{A3}$$

To transform to the Tchebichef form, introduce the dimensionless coordinate, ξ:

$$\xi = \frac{x}{l/2} = \cos \varphi, \qquad -1 \le \xi \le 1 \tag{A4}$$

Introducing the Tchebichef polynomials, reference 6,

$$\left.\begin{aligned} T_n(\xi) &= \cos n\varphi \\ V_n(\xi) &= \frac{\sin n\varphi}{\sin \varphi} \equiv U_{n-1}(\xi) \end{aligned}\right\} n=0,1,2, \ldots \tag{A5}$$

one may write equation (A3) as

$$A_n = \frac{4}{\pi l}\int_{-1}^{1} \frac{dS}{d\xi} V_n(\xi) d\xi, \qquad n=1,2,3, \ldots \tag{A6}$$

(A summary of the theory and properties of the Tchebichef polynomials is given at the end of this appendix.) Due to the fact that $V_n(-\xi) = (-1)^{n-1}V_n(\xi)$, equation (A40), equation (A6) can be simplified to

$$A_n = \frac{4}{\pi l}\int_0^1 V_n(\xi)\frac{d}{d\xi}\left[S(\xi) + (-1)^n S(-\xi)\right]d\xi \tag{A7}$$

Since $V_1(\xi) = 1$, from the definition, equation (A5), the first coefficient, A_1, can be computed immediately:

$$A_1 = \frac{4}{\pi l}\left[S(1) - S(-1)\right] \tag{A8}$$

Henceforth A_n will be considered only for the positive integral values of $n = 2, 3, 4, \ldots$.

In the next section general numerical integration formulas will be developed, and in the following section they will be applied to equation (A7).

General Integration Procedure

The general problem of the numerical evaluation of integrals of the type

$$\int_a^b f(\xi)g(\xi)d\xi$$

has been discussed by Sheldon in reference 14, and the particular case in which $g(\xi)$ is a trigonometric function has been treated by Filon in reference 15. Here the problem is generalized to include any derivative of $f(\xi)$ rather than just the function itself. The so-called "strip method" is used, in which the range of integration is broken into N strips of equal length, and $f(\xi)$ is approximated in each strip by a polynomial. Thus

$$\int_a^b f(\xi)g(\xi)d\xi = \sum_{k=0}^{N-1}\int_{a_k}^{a_{k+1}} f(\xi)g(\xi)d\xi \tag{A9}$$

where $a_0 = a, a_1, a_2, \ldots, a_{N-1}, a_N = b$ are the boundary points of the N strips. The integral over each strip is evaluated by approximating $f(\xi)$ by a polynomial of degree m and subdividing the strip into m

[redacted]

intervals of length Δ, this interval length being constant throughout the entire range (a,b). Thus, the lattice points within the kth strip are a_k, $a_k + \Delta$, . . ., $a_k + m\Delta = a_{k+1}$. Since the case of most interest is that in which $f(\xi)$ represents experimental data, it is assumed that $f(\xi)$ is not known continuously but only at these lattice points. Hence it is desired to obtain an integration formula involving only these points:

$$\int_{a_k}^{a_{k+1}} f(\xi)g(\xi)d\xi = \sum_{j=0}^{m} \alpha(m,j,k)f(a_k + j\Delta) \tag{A10}$$

where the coefficients $\alpha(m,j,k)$ are to be determined as functions of $g(\xi)$. Substituting equation (A10) in (A9) gives

$$\int_{a}^{b} f(\xi)g(\xi)d\xi = \sum_{k=0}^{N-1} \sum_{j=0}^{m} \alpha(m,j,k)f(a_k + j\Delta) \tag{A11}$$

If all the lattice points are numbered consecutively over the entire range, $a = \xi_0, \xi_1, \xi_2, \ldots, \xi_{Nm} = b$, then

$$\xi_{km+j} = a_k + j\Delta$$

and rearrangement of equation (A11) gives

$$\int_{a}^{b} f(\xi)g(\xi)d\xi = \sum_{r=0}^{Nm} \mu(m,r)f(\xi_r) \tag{A12}$$

where the μ's are just the α's suitably renumbered, except that the μ corresponding to each strip boundary point contains two α's, one being the last α for the left-hand strip and the other being the first α for the right-hand strip, thus:

$$\left.\begin{aligned} \mu(m,0) &= \alpha(m,0,0) \\ \mu(m,km) &= \alpha(m,0,k) + \alpha(m,m,k-1) \qquad k=1,2,3, \ldots, N-1 \\ \mu(m,km+j) &= \alpha(m,j,k), \qquad k=0,1, \ldots, N-1 \quad j=1,2, \ldots, m-1 \\ \mu(m,Nm) &= \alpha(m,m,N-1) \end{aligned}\right\} \tag{A13}$$

Thus equation (A12) is the desired integration formula, the coefficients μ being given by equation (A13), while the coefficients α are implicitly defined by equation (A10). It remains to determine them explicitly. This is done by requiring that equation (A10) be exact whenever $f(\xi)$ is a polynomial of degree m. (It must be remembered that all numerical integration formulas are approximations when the integrands are arbitrary.) This is equivalent to requiring that equation (A10) be exact for any set of $m + 1$ linearly independent polynomials of degree m. The most convenient choice is the set of Lagrangian interpolation polynomials $L(m,j,k;\xi)$ defined by (ref. 16):

$$L(m,j,k;a_k + r\Delta) = \begin{cases} 0 & \text{if } r \neq j \\ 1 & \text{if } r = j \end{cases} \tag{A14}$$

An explicit representation is

$$\begin{aligned} L(m,j,k;\xi) &= \prod_{\substack{i=0 \\ i\neq j}}^{m} \frac{\xi - (a_k + i\Delta)}{a_k + j\Delta - (a_k + i\Delta)} \\ &= \frac{(-1)^{m-j}}{j!(m-j)!\Delta^m} \prod_{\substack{i=0 \\ i\neq j}}^{m} (\xi - \xi_{km+i}) \end{aligned} \tag{A15}$$

Substituting $L(m,j,k;\xi)$ for $f(\xi)$ in equation (A10) gives, by virtue of equation (A14) the explicit formula for the α:

$$\alpha(m,j,k) = \int_{a_k}^{a_{k+1}} L(m,j,k;\xi)g(\xi)d\xi \tag{A16}$$

More generally, if it is desired to evaluate an integral involving not $f(\xi)$ but any one of its derivatives,

$$\int_a^b \frac{d^r f(\xi)}{d\xi^r} g(\xi)d\xi$$

then formulas (A10) through (A16) remain valid, except that in (A16) L must be replaced by the corresponding derivative

$$\frac{d^r L(m,j,k;\xi)}{d\xi^r}$$

while f is replaced by the derivative in the integrands but <u>not</u> in the sums.

Clearly the effectiveness of this entire procedure hinges upon the difficulty of calculating the α from equation (A16). To estimate this difficulty it is worthwhile exhibiting some of the L's explicitly; the second form of equation (A15) gives, for $m = 1, 2, 3$, respectively:

$$\left.\begin{aligned} L(1,0,k;\xi) &= -\frac{1}{\Delta}(\xi - \xi_{k+1}) \\ L(1,1,k;\xi) &= \frac{1}{\Delta}(\xi - \xi_{k}) \end{aligned}\right\} \tag{A17}$$

$$\left.\begin{aligned} L(2,0,k;\xi) &= \frac{1}{2\Delta^2}(\xi - \xi_{2k+1})(\xi - \xi_{2k+2}) \\ L(2,1,k;\xi) &= -\frac{1}{\Delta^2}(\xi - \xi_{2k})(\xi - \xi_{2k+2}) \\ L(2,2,k;\xi) &= \frac{1}{2\Delta^2}(\xi - \xi_{2k})(\xi - \xi_{2k+1}) \end{aligned}\right\} \tag{A18}$$

$$\left.\begin{aligned} L(3,0,k;\xi) &= \frac{-1}{6\Delta^3}(\xi - \xi_{3k+1})(\xi - \xi_{3k+2})(\xi - \xi_{3k+3}) \\ L(3,1,k;\xi) &= \frac{1}{2\Delta^3}(\xi - \xi_{3k})(\xi - \xi_{3k+2})(\xi - \xi_{3k+3}) \\ L(3,2,k;\xi) &= \frac{-1}{2\Delta^3}(\xi - \xi_{3k})(\xi - \xi_{3k+1})(\xi - \xi_{3k+3}) \\ L(3,3,k;\xi) &= \frac{1}{6\Delta^3}(\xi - \xi_{3k})(\xi - \xi_{3k+1})(\xi - \xi_{3k+2}) \end{aligned}\right\} \tag{A19}$$

It is a straightforward, though tedious, task to extend such a table to as high a degree, m, as is desired. The calculation of the integral in equation (A16) then depends on the nature of the function $g(\xi)$. This calculation can be performed analytically whenever $g(\xi)$ is a polynomial, trigonometric, hyperbolic, exponential, or logarithmic function. For more complicated functions, $g(\xi)$, it may be necessary to resort to numerical integration at this stage, which <u>almost</u> defeats the purpose of the entire procedure! However, these integrations (eq. (A16)) are performed only once, and then equations (A12) and (A13) are applicable to arbitrary functions $f(\xi)$. In the next section, then, these results will be applied to the integrals of equation (A7).

Tchebichef Integration Coefficients

Writing equation (A7) in the form of the preceding section,

$$A_n = \frac{4}{\pi l} \int_0^1 \frac{dS_n(\xi)}{d\xi} V_n(\xi) d\xi \tag{A20}$$

with

$$S_n(\xi) = S(\xi) + (-1)^n S(-\xi) \tag{A21}$$

the desired result is, analogous to equation (A12),

$$A_n = \frac{1}{l} \sum_{r=0}^{M} \mu_{nr} S_n(\xi_r) \tag{A22}$$

where $M = mN$, the subscript m has been dropped for brevity, while the subscript n has been added for clarity. The μ's are still given by equations (A13), but (A16) now becomes

$$\alpha(m,j,k) = \int_{a_k}^{a_{k+1}} V_n(\xi) \frac{dL(m,j,k;\xi)}{d\xi} d\xi \tag{A23}$$

These will now be integrated explicity for the linear ($m = 1$) and quadratic ($m = 2$) cases.

Linear approximation.- In the linear case each strip consists of a single interval of width Δ, $m = 1$, $a_k = \xi_k = k\Delta$, $M = N$, $N\Delta = 1$, and the derivatives of the Lagrangian interpolation polynomials are, from equation (A17)

$$\frac{dL(1,0,k;\xi)}{d\xi} = \frac{-1}{\Delta} ; \qquad \frac{dL(1,1,k;\xi)}{d\xi} = \frac{1}{\Delta}$$

Substitution in equation (A23) gives, for $j = 0,1$, respectively,

$$\left.\begin{aligned} \alpha(1,0,k) &= \frac{-1}{\Delta} \int_{\xi_k}^{\xi_{k+1}} V_n(\xi) d\xi \\ \alpha(1,1,k) &= \frac{1}{\Delta} \int_{\xi_k}^{\xi_{k+1}} V_n(\xi) d\xi \end{aligned}\right\} \tag{A24}$$

[redacted]

Now, by equation (A44), $V_n = \frac{1}{n}\frac{dT_n}{d\xi}$, and therefore equation (A24) can be integrated directly to give

$$\alpha(1,0,k) = \frac{1}{n\Delta}\left[T_n(\xi_k) - T_n(\xi_{k+1})\right]$$

$$\alpha(1,1,k) = \frac{1}{n\Delta}\left[T_n(\xi_{k+1}) - T_n(\xi_k)\right]$$

Substituting these in equation (A13) and changing the notation to agree with equation (A22) gives

$$\left.\begin{aligned}
\mu_{no} &= \frac{4}{\pi n\Delta}\left[T_n(0) - T_n(\Delta)\right] \\
\mu_{nr} &= \frac{4}{\pi n\Delta}\left[-T_n(\xi_{r-1}) + 2T_n(\xi_r) - T_n(\xi_{r+1})\right], \quad r=1,2, \ldots,N-1 \\
\mu_{nN} &= \frac{4}{\pi n\Delta}\left[T_n(1) - T_n(1-\Delta)\right]
\end{aligned}\right\} \quad (A25)$$

In the linear case, then, the complete solution is given by equations (A21), (A22), and (A25).

Quadratic approximation.- In the quadratic case, each strip consists of two intervals, each of width Δ, $m = 2$, $M = 2N$, $a_k = \xi_{2k} = 2k\Delta$, $2N\Delta = 1$, and the derivatives of the Lagrangian interpolation polynomials are, from equation (A18),

$$\frac{dL(2,0,k;\xi)}{d\xi} = \frac{2\xi - (4k+3)\Delta}{2\Delta^2}$$

$$\frac{dL(2,1,k;\xi)}{d\xi} = \frac{(4k+2)\Delta - 2\xi}{\Delta^2}$$

$$\frac{dL(2,2,k;\xi)}{d\xi} = \frac{2\xi - (4k+1)\Delta}{2\Delta^2}$$

Substitution in equation (A23) gives, for $j = 0,1,2$, respectively,

$$\left.\begin{aligned}
\alpha(2,0,k) &= \int_{\xi_{2k}}^{\xi_{2k+2}} \frac{2\xi - (4k+3)\Delta}{2\Delta^2} V_n(\xi)d\xi \\
\alpha(2,1,k) &= \int_{\xi_{2k}}^{\xi_{2k+2}} \frac{(4k+2)\Delta - 2\xi}{\Delta^2} V_n(\xi)d\xi \\
\alpha(2,2,k) &= \int_{\xi_{2k}}^{\xi_{2k+2}} \frac{2\xi - (4k+1)\Delta}{2\Delta^2} V_n(\xi)d\xi
\end{aligned}\right\} \tag{A26}$$

Now, from equation (A42),

$$2\xi V_n(\xi) = V_{n+1}(\xi) + V_{n-1}(\xi)$$

and, as before, $V_n = \frac{1}{n}\frac{dT_n}{d\xi}$. If these relations are substituted in equation (A26), the integrations can be performed immediately to give

$$\left.\begin{aligned}
\alpha(2,0,k) &= \frac{1}{2\Delta^2}\left[W(n+1,k) + W(r-1,k) - (4k+3)W(r,k)\Delta\right] \\
\alpha(2,1,k) &= \frac{1}{\Delta^2}\left[(4k+2)W(n,k)\Delta - W(n+1,k) - W(n-1,k)\right] \\
\alpha(2,2,k) &= \frac{1}{2\Delta^2}\left[W(n+1,k) + W(n-1,k) - (4k+1)W(n,k)\Delta\right]
\end{aligned}\right\} \tag{A27}$$

where

$$W(n,k) = \frac{T_n(\xi_{2k+2}) - T_n(\xi_{2k})}{n} \tag{A28}$$

For this case equation (A13) becomes, in the notation of equation (A22):

$$\left.\begin{aligned}
\mu_{n,0} &= \frac{4}{\pi}\alpha(2,0,0) \\
\mu_{n,2r} &= \frac{4}{\pi}\alpha(2,0,r) + \frac{4}{\pi}\alpha(2,2,r-1) \\
\mu_{n,2r+1} &= \frac{4}{\pi}\alpha(2,1,r),\ r=0,1,\ \ldots,N-1 \\
\mu_{n,2N} &= \frac{4}{\pi}\alpha(2,2,N-1)
\end{aligned}\right\} \tag{A29}$$

In the quadratic case, then, the complete solution is given by equations (A21), (A22), and (A27) to (A29).

It is clear from equations (A15) and (A23) that in order to use higher degree approximating polynomials, it is necessary to evaluate integrals of the type

$$\int_{\xi_{km}}^{\xi_{k(m+1)}} \xi^j V_n(\xi)\,d\xi$$

for successive values of $j = 0, 1, 2, \ldots, m - 1$. While no explicit formulas will be given, the section "Theory and Properties of Tchebichef Polynomials" does include some recurrence relations which can be used in an obvious way to perform such integrations systematically for successive values of j. In every case the results, α and μ, involve only the one kind of Tchebichef polynomials $T_n(\xi)$, $T_{n+1}(\xi)$, etc.

Numerical tables of the integration coefficients μ_{nr} have been constructed, by the procedures discussed below, for the linear and quadratic cases.

Checking Procedure

In any lengthy numerical calculation it is desirable to have a checking procedure, even if it merely consists of repeating the calculation. In the present case it is possible to do much better than this. Once the Fourier coefficients, A_n, have been calculated, they can be used in a reverse sense to calculate the area distribution, $S(\xi)$, which can be compared with the original data as a check. This is a quite effective check, since it detects any of the following: errors in the theory itself, errors in the tables of integration coefficients, errors in reading graphical data, errors due to using too few terms of the Fourier series (eq. (A2)), round-off errors, and errors made by the computing machine or human operator. Clearly, such an independent checking procedure is preferable to a mere repetition of the direct calculation, which would only detect machine or operator errors.

Such a check is easily derived from equation (A2). Transforming to the variable ξ by means of equations (A4) and (A5) gives

$$\frac{dS}{d\xi} = \frac{1}{2}\sum_{n=1}^{\infty} A_n V_n(\xi)\sqrt{1-\xi^2} \tag{A30}$$

From equation (A45),

$$V_n(\xi)\sqrt{1-\xi^2} = \frac{d}{d\xi}\left\{\frac{1}{2}\sqrt{1-\xi^2}\left[\frac{V_{n+1}(\xi)}{n+1} - \frac{V_{n-1}(\xi)}{n-1}\right]\right\}, \quad n=2,3, \ldots$$

while, since $V_1(\xi) = 1$,

$$V_1(\xi)\sqrt{1-\xi^2} = \frac{d}{d\xi}\left(\frac{1}{2}\xi\sqrt{1-\xi^2} + \frac{1}{2}\arcsin\xi\right)$$

Substituting these in equation (A30) gives

$$\frac{dS}{d\xi} = \frac{l}{4}\frac{d}{d\xi}\left\{\left(\xi\sqrt{1-\xi^2} + \arcsin\xi\right)A_1 + \sum_{n=2}^{\infty}\sqrt{1-\xi^2}\left[\frac{V_{n+1}(\xi)}{n+1} - \frac{V_{n-1}(\xi)}{n-1}\right]A_n\right\} \tag{A31}$$

and $S(\xi)$ can be obtained immediately.

$$S(\xi) = C + \frac{l}{4}\left(\xi\sqrt{1-\xi^2} + \arcsin\xi\right)A_1 + \frac{l}{4}\sqrt{1-\xi^2}\sum_{n=2}^{\infty}A_n\left[\frac{V_{n+1}(\xi)}{n+1} - \frac{V_{n-1}(\xi)}{n-1}\right] \tag{A32}$$

where C is a constant of integration. Setting $\xi = 1$ gives

$$S(1) = C + \frac{\pi l}{8}A_1$$

Eliminating C in equation (A32) gives

$$S(\xi) = S(1) + \frac{l}{4}\left(\xi\sqrt{1-\xi^2} - \arccos\xi\right)A_1 + \frac{l}{4}\sqrt{1-\xi^2}\sum_{n=2}^{\infty}A_n\left[\frac{V_{n+1}(\xi)}{n+1} - \frac{V_{n-1}(\xi)}{n-1}\right] \tag{A33}$$

It is also convenient to set $\xi = -1$ in equation (A32), giving

$$S(-1) = C - \frac{\pi l}{8}A_1$$

[redacted]

Using this to eliminate C in equation (A32) and then substituting $-\xi$ for ξ gives

$$S(-\xi) = S(-1) - \frac{1}{4}\left(\xi\sqrt{1-\xi^2} - \arccos \xi\right)A_1 + \frac{1}{4}\sqrt{1-\xi^2}\sum_{n=2}^{\infty}(-1)^n A_n\left[\frac{V_{n+1}(\xi)}{n+1} - \frac{V_{n-1}(\xi)}{n-1}\right] \qquad (A34)$$

by virtue of equation (A40). Equation (A33) is used as a check for positive values of ξ and (A34) for negative values. They can be written more briefly as

$$S(\pm\xi) = S(\pm 1) + 1\sum_{n=1}^{\infty}(\pm 1)^n C_n(\xi)A_n \qquad 0 \le \xi \le 1 \qquad (A35)$$

where

$$\left.\begin{aligned} C_1(\xi) &= \frac{1}{4}\left(\xi\sqrt{1-\xi^2} - \arccos \xi\right) \\ C_n(\xi) &= \frac{1}{4}\sqrt{1-\xi^2}\left[\frac{V_{n+1}(\xi)}{n+1} - \frac{V_{n-1}(\xi)}{n-1}\right], \quad n=2,3,4, \ldots \end{aligned}\right\} \qquad (A36)$$

and in (A35) either the upper or lower sign is to be used throughout. It should be emphasized that equations (A35) and (A36) constitute a check regardless of the choice of any particular method of computing the Fourier coefficients, A_n.

Construction and Checking of Tables

The usefulness of the present theory lies in the fact that it makes possible the construction of numerical tables of the integration coefficients, μ_{nr}, equations (A25) and (A29), and of the check coefficients, $C_n(\xi)$, equation (A36). Once such tables have been prepared, the calculation of the Fourier coefficients, A_n, from equation (A22) and the checking by means of equation (A35) is a straightforward, systematic, arithmetical procedure, whether or not automatic computing machinery is available. Such tables of coefficients have been computed (and are available on punched data cards upon request) for integral values of n from 1 to 98, and for ξ in the range of 0 to 1 at an interval of 0.01. All these calculations were performed on an IBM type 605 Electronic Calculating Punch. Fixed-decimal, 13-digit arithmetic was used, and the final values of the

coefficients μ_{nr} and $C_n(\xi)$ were rounded off to 10 digits to be in a form suitable for use in magnetic-drum calculators. The sequence of calculations was as follows (see next section for proofs):

a. $T_0(\xi) = 1$, $T_1(\xi) = \xi$

b. $T_{n+1}(\xi) = 2\xi T_n(\xi) - T_{n-1}(\xi)$, $n = 1,2,3,\ldots,99$

c. $V_0(\xi) = 0$, $V_1(\xi) = 1$

d. $V_{n+1}(\xi) = 2\xi V_n(\xi) - V_{n-1}(\xi)$, $n = 1,2,3,\ldots,99$

e. $C_n(\xi)$ was then computed using equation (A36) with $n = 1,2,3,\ldots,98$, $\xi = 0.00, 0.01, 0.02,\ldots,0.99, 1.00$

f. $T_n(\xi) - T_n(\xi - 0.01)$ was computed for $n = 0,1,2,\ldots,99$, $\xi = 0.01, 0.02,\ldots,1.00$

g. $\mu_{nr}(n = 2,3,\ldots,98,\ r = 0,1,\ldots,100)$ was computed for the linear case from equations (A25).

h. $W(n,k)$ was computed for $n = 1,2,\ldots,99$, $k = 0,1,\ldots,49$ from equation (A28)

i. $\alpha(2,j,k)$ was computed for $j = 0,1,2$, $k = 0,1,2,\ldots,49$ from equation (A27)

j. $\mu_{nr}(n = 2,3,\ldots,98;\ r = 0,1,\ldots,100)$ was computed for the quadratic case from equation (A29)

As a preliminary check, the tables of $T_n(\xi)$ and $V_n(\xi)$ were checked using equations (A43):

$$\left.\begin{aligned} T_{n+1}(\xi) &= \xi T_n(\xi) - (1 - \xi^2)V_n(\xi) \\ V_{n+1}(\xi) &= \xi V_n(\xi) + T_n(\xi) \end{aligned}\right\} n=0,1,\ldots,98$$

The tables of μ_{nr} were checked as follows: For the linear case, the integration formula (A22) should be exact if $S(\xi)$ is linear. That is, equations (A20) and (A22) should give the same results for the Fourier coefficients, A_n, whenever $S(\xi)$ is linear. This check was applied for various linear functions $S(\xi)$. For the quadratic case, equations (A20) and (A22) should give the same result for the Fourier coefficients, A_n, whenever $S(\xi)$ is linear or quadratic. This check was applied for various linear and quadratic functions $S(\xi)$.

The tables of check coefficients, $C_n(\xi)$, were checked by constructing analytic functions $S(\xi)$ having only a finite number of nonvanishing

Fourier coefficients, A_n, all of which were calculated analytically and then substituted in the check equation (A35).

The purpose of these checks is to ensure that all the tables are free of numerical errors. There still remains the question of two other sources of error: the approximation of $S(\xi)$ by a polynomial, and the use of only a finite number of terms A_n. These two effects are discussed in the main body of the present report, particularly in connection with the Sears-Haack body. In general, such questions can only be examined empirically. If the check procedure indicates the presence of errors, three things can be done. More coefficients A_n can be taken, a finer interval Δ can be used, or higher degree polynomial approximation can be used. Any of these courses of action requires extending the basic tables. In many practical cases the data function $S(\xi)$ is originally obtained by fairing a curve through a reasonable number of points. Obviously, the use of a finer reading interval Δ is incapable of yielding greater accuracy in such cases. Use of higher degree polynomials is sometimes justified, but this also can give illusory improvements. For example, a curve with sharp changes in slope is better approximated by short straight-line segments than by longer arcs of higher degree polynomials. Finally, the use of more terms in the Fourier series can be reduced to an absurdity once the wave lengths involved become shorter than the reading interval Δ.

Theory and Properties of Tchebichef Polynomials

The Tchebichef polynomials are defined in reference 6 as

$$\left.\begin{aligned} T_n(\xi) &= \cos n\varphi \\ U_n(\xi) &= [\sin(n+1)\varphi]/\sin\varphi \end{aligned}\right\} \tag{A37}$$

where $\xi = \cos\varphi$. Since $U_{n-1}(\xi)$ is closely related to the Fourier coefficient, A_n, it seems convenient to introduce the notation

$$V_n(\xi) = U_{n-1}(\xi) = \frac{\sin n\varphi}{\sin\varphi} \tag{A38}$$

Since the principal properties of these polynomials, including the fact that they are polynomials in ξ, are treated extensively in reference 6, the present section will list and prove only those that have been used in this report.

First, the following are obvious from the definitions:

$$T_0(\xi) = 1, \quad T_1(\xi) = \xi, \quad V_0(\xi) = 0, \quad V_1(\xi) = 1 \tag{A39}$$

Next consider the effect of replacing ξ by $-\xi$, so that φ is replaced by $\pi - \varphi$, that is, $\cos(\pi - \varphi) = -\cos\varphi$:

$$T_n(-\xi) = \cos n(\pi - \varphi) = \cos n\pi \cos n\varphi$$

$$V_n(-\xi) = \frac{\sin n(\pi - \varphi)}{\sin(\pi - \varphi)} = \frac{-\cos n\pi \sin n\varphi}{-\cos \pi \sin \varphi}$$

Thus

$$T_n(-\xi) = (-1)^n T_n(\xi), \qquad V_n(-\xi) = (-1)^{n-1} V_n(\xi) \tag{A40}$$

for all integral values of n.

Next, setting $\xi = 1$ gives $\varphi = 0$, $T_n = 1$, while V_n is the indeterminate form

$$\lim_{\varphi \to 0} \frac{\sin n\varphi}{\sin \varphi}$$

Applying L'Hospital's rule gives

$$T_n(1) = 1, \qquad V_n(1) = n \tag{A41}$$

Recurrence relations can be obtained directly from the definitions using the trigonometric addition formulas

$$\sin(a \pm b) = \sin a \cos b \pm \cos a \sin b$$

$$\cos(a \mp b) = \cos a \cos b \pm \sin a \sin b$$

By use of these, the following are easily proved:

$$\left.\begin{aligned} T_{n+1}(\xi) &= 2\xi T_n(\xi) - T_{n-1}(\xi) \\ V_{n+1}(\xi) &= 2\xi V_n(\xi) - V_{n-1}(\xi) \end{aligned}\right\} \tag{A42}$$

and

$$\left.\begin{aligned} T_{n+1}(\xi) &= \xi T_n(\xi) - (1 - \xi^2) V_n(\xi) \\ V_{n+1}(\xi) &= \xi V_n(\xi) + T_n(\xi) \end{aligned}\right\} \tag{A43}$$

Numerous differential and integral identities are obtainable, analogous to the trigonometrical formulas

$$\frac{d \sin \psi}{d\psi} = \cos \psi, \qquad \frac{d \cos \psi}{d\psi} = -\sin \psi$$

For example, differentiating the definition of ξ gives

$$\frac{d\xi}{d\varphi} = -\sin\varphi = -\sqrt{1-\xi^2}$$

Thus, differentiating $T_n(\xi)$, equation (A37), gives

$$\frac{dT_n}{d\xi} = \frac{dT_n/d\varphi}{d\xi/d\varphi} = \frac{-n \sin n\varphi}{-\sin\varphi}$$

that is

$$\frac{dT_n(\xi)}{d\xi} = nV_n(\xi) \tag{A44}$$

Next consider

$$\frac{d}{d\xi}\left\{\frac{1}{2}\sqrt{1-\xi^2}\left[\frac{V_{n+1}(\xi)}{n+1} - \frac{V_{n-1}(\xi)}{n-1}\right]\right\} = \frac{d}{d\xi}\left\{\frac{1}{2}\left[\frac{\sin(n+1)\varphi}{n+1} - \frac{\sin(n-1)\varphi}{n-1}\right]\right\}$$

$$= \frac{1}{2}\left[\cos(n+1)\varphi - \cos(n-1)\varphi\right]\frac{d\varphi}{d\xi}$$

$$= \frac{-\sin n\varphi \sin\varphi}{-\sin\varphi} = V_n \sin\varphi$$

that is

$$\frac{d}{d\xi}\left\{\frac{1}{2}\sqrt{1-\xi^2}\left[\frac{V_{n+1}(\xi)}{n+1} - \frac{V_{n-1}(\xi)}{n-1}\right]\right\} = V_n(\xi)\sqrt{1-\xi^2} \tag{A45}$$

Finally, to evaluate integrals of the type (see above)

$$I(j,n) \equiv \int \xi^j V_n(\xi)\,d\xi \tag{A46}$$

consider first the case $j = 0$. This can be integrated immediately by virtue of equation (A44) to give

$$I(0,n) = \frac{1}{n} T_n(\xi) \tag{A47}$$

Next, if $j \geq 1$, use the recurrence relation (A42) to write

$$I(j,n) = \int \xi^{j-1}\xi V_n d\xi = \frac{1}{2}\int \xi^{j-1}\left[V_{n+1}(\xi) + V_{n-1}(\xi)\right]d\xi$$

that is

$$I(j,n) = \frac{1}{2}\left[I(j-1,n-1) + I(j-1,n+1)\right] \tag{A48}$$

Thus, from equation (A47), $I(0,n)$ can be evaluated for $n = 1,2, \ldots$. Then from equation (A48), $I(j,n)$ can be obtained by recurrence, using the one additional equation

$$I(j,0) = 0 \tag{A49}$$

since $V_0(\xi) \equiv 0$.

By means of these equations the integrals $I(j,n)$ can be evaluated systematically, either analytically or numerically. The general integration procedure presented above can then be applied to extend the Tchebichef integration coefficients to any desired degree of polynomial approximation.

REFERENCES

1. Holdaway, George H.: Comparison of Theoretical and Experimental Zero-Lift Drag-Rise Characteristics of Wing-Body-Tail Combinations Near the Speed of Sound. NACA RM A53H17, 1953.

2. Carmel, Melvin M.: An Experimental Transonic Investigation of a 45° Sweptback Wing-Body Combination With Several Types of Body Indentation With Theoretical Comparisons Included. NACA RM L54I07a, 1954.

3. Holdaway, George H.: Additional Comparisons Between Computed and Measured Transonic Drag-Rise Coefficients at Zero Lift for Wing-Body-Tail Configurations. NACA RM A55F06, 1955.

4. Hoffman, Sherwood, Wolff, Austin L., and Faget, Maxime A.: Flight Investigation of the Supersonic Area Rule for a Straight Wing-Body Configuration at Mach Numbers Between 0.8 and 1.5. NACA RM L55C09, 1955.

5. Jones, Robert T.: Theory of Wing-Body Drag at Supersonic Speeds. NACA RM A53H18a, 1953.

6. Erdélyi, Arthur, Magnus, Wilhelm, Oberhettinger, Fritz, and Tricomi, Francesco G.: Higher Transcendental Functions, vol. 2, McGraw-Hill Book Co., 1953, pp. 183-188.

7. U. S. Nat. Bur. of Standards: Tables of Chebyshev Polynomials $S_n(X)$ and $C_n(X)$. (Appl. Math. Ser., vol. 9.) U. S. Gov't. Print. Office, Washington, 1952.

8. Carslaw, H. S.: Introduction to the Theory of Fourier's Series and Integrals. Third ed., Dover Pub., Inc., 1930.

9. Kehlet, Alan B.: Aerodynamic Characteristics at Transonic and Supersonic Speeds of a Rocket-Propelled Airplane Configuration Having a 52.5° Delta Wing and a Low, Swept Horizontal Tail. NACA RM L54A20, 1954.

10. Hayes, W. S., and Shutte, R. H.: Zero-Lift Drag Predictions for Nike 484, Nike 490, and Nike I Missiles. Rep. No. SM-14130, Douglas Aircraft Co., Inc., Santa Monica, Aug. 13, 1953.

11. Blanchard, Willard S., Jr.: A Summary of the Low-Lift Drag and Longitudinal Trim Characteristics of Two Versions of an Interceptor-Type Airplane as Determined from Flight Tests of Rocket-Powered Models at Mach Numbers Between 0.75 and 1.78. NACA RM L54H31, 1954.

[redacted]

12. Selna, James: Preliminary Investigation of a Submerged Inlet and a Nose Inlet in the Transonic Flight Range With Free-Fall Models. NACA RM A51B14, 1951.

13. Sears, R. I., and Merlet, C. F.: Flight Determination of the Drag and Pressure Recovery of an NACA 1-40-250 Nose Inlet at Mach Numbers from 0.9 to 1.8. NACA RM L50L18, 1951.

14. Sheldon, John W.: Numerical Evaluation of Integrals of the Form $\int_{\alpha}^{\beta} f(x)g(x)dx$. Proceedings, Industrial Computation Seminar. International Business Machines Corporation, New York, Sept. 1950, pp. 74-77.

15. Filon, L. N. G.: On a Quadrature Formula for Trigonometric Integrals. Proc. Roy. Soc., Edinburgh, vol. 49, 1928-9, pp. 38-47.

16. Milne, W. E.: Numerical Calculus. Princeton Univ. Press, 1949, p. 83.

TABLE I.- HARMONIC SOLUTION FOR A FINENESS RATIO 12.5 SEARS-HAACK BODY BY TCHEBICHEF POLYNOMIALS

n	Linear approximation[1] A_n	Linear approximation[1] $\sum_{n=1}^{N} nA_n^2$	Quadratic approximation[1] $\sum_{n=1}^{N} nA_n^2$
1	0.00000	0.000	0.000
2	-10.16125	206.502	206.504
3	.00000	206.502	206.504
4	.00091	206.502	206.504
5	.00000	206.502	206.504
6	-.00091	206.502	206.504
7	.00000	206.502	206.504
8	-.00821	206.502	206.504
9	.00000	206.502	206.504
10	-.01982	206.506	206.505
11	.00000	206.506	206.505
12	-.02552	206.514	206.506
13	.00000	206.514	206.506
14	-.02876	206.525	206.506
15	.00000	206.525	206.506
16	-.02313	206.534	206.507
17	.00000	206.534	206.507
18	-.02113	206.542	206.508
19	.00000	206.542	206.508
20	-.04124	206.576	206.511
21	.00000	206.576	206.511
22	-.03279	206.599	206.524
23	.00000	206.599	206.524
24	-.07421	206.731	206.548
25	.00000	206.731	206.548

[1]Methods used in approximating $S(\xi)$, see the appendix.

The theoretical solution for this body is:

$$\sum_{n=1}^{\infty} nA_n^2 = 2A_2^2 = 206.521 \text{ sq in.}$$

TABLE II.- TCHEBICHEF SOLUTION FOR AN AREA CURVE WITH A DISCONTINUITY OF SLOPE

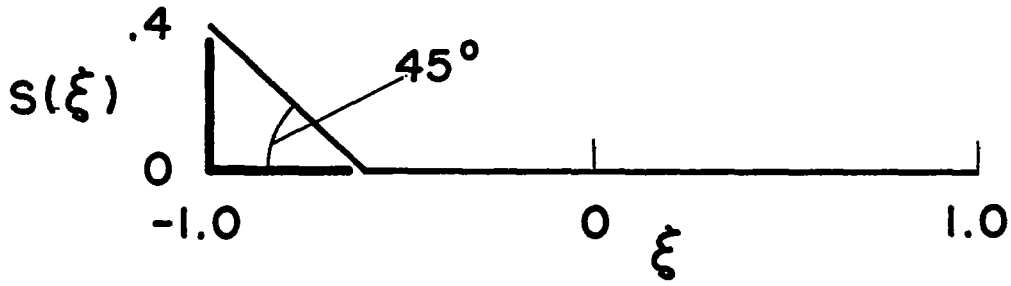

n	$A_n = -\frac{4}{n^2\pi}\left[T_n\right]_{-1.0}^{-0.6}$	A_n(machine computed)[1]
1	-0.254648	-0.254648
2	.407437	.407438
3	-.410832	-.410837
4	.293354	.293359
5	-.136980	-.136983
6	.026293	.026296
7	-.001958	-.001961
8	.045998	.045999
9	-.104130	-.104131
10	.126592	.126594
11	-.099202	-.099202
12	.046071	.046071
13	-.006268	-.006269
14	.003874	.003874
15	-.032859	-.032858
16	.065408	.065407
17	-.074838	-.074839
18	.054970	.054970
19	-.022337	-.022337
20	.001456	.001456
21	-.005707	-.005707
22	.028363	.028362
23	-.049488	-.049490
24	.052133	.052133
25	-.034900	-.034900

[1]Machine computation, linear approximation of $S(\xi)$, see the appendix.

TABLE III.- COMPARISON OF TCHEBICHEF SOLUTIONS WITH VALUES COMPUTED BY THE METHOD OF REFERENCE 1 FOR A BASIC SWEPT-WING MODEL (REF. 3)

Area Curve				
	$M=1.5$, $\theta=90^\circ$, $\Psi=0^\circ$		$M=1.5$, $\theta=22.5^\circ$, $\Psi=46.0^\circ$	
N	Tchebichef $\sum_{n=1}^{N} nA_n^2$	Method of ref. 1 $\sum_{n=1}^{N} nA_n^2$	Tchebichef $\sum_{n=1}^{N} nA_n^2$	Method of ref. 1 $\sum_{n=1}^{N} nA_n^2$
1	0	0	0	0
2	282	277	278	272
3	283	277	278	272
4	315	315	284	284
5	316	317	290	289
6	405	390	291	290
7	414	396	322	320
8	521	513	326	326
9	529	524	344	349
10	628	610	385	393
11	643	624	386	393
12	686	676	483	480
13	703	692	493	496
14	722	708	533	552
15	729	717	588	602
16	729	717	598	605
17	732	721	649	663
18	736	724	660	676
19	737	725	680	695
20	749	736	712	726
21	750	736	713	729
22	757	744	738	754
23	759	744	759	781
24	763	748	759	781
25	764		783	
	No discontinuity of slope. Difference ~ 2 percent		Discontinuity of slope. Difference ~ 3 percent	

See figure 4 for plots of Tchebichef check solutions.

TABLE IV.- FUSELAGE ORDINATES OF BASIC BODY - MODEL 3

Fuselage station, in.	Radius, in.
0	0.28
5.00	1.46
10.00	2.41
20.00	3.90
30.00	5.07
40.00	6.01
50.00	6.78
60.00	7.40
70.00	7.86
80.00	8.20
90.00	8.41
102.00	8.50
110.00	8.46
120.00	8.30
130.00	7.99
140.00	7.67
150.00	7.36
160.00	7.10
170.00	6.70
180.00	6.27
190.00	5.77
200.00	5.25
210.00	4.50
219.00	2.32
225.38	0

[redacted]

TABLE V.- FUSELAGE ORDINATES OF SCOOP BODY - MODEL 3
[All dimensions given in inches.]

Station	Dimensions				
	r	W	X	Y	Z
25.00	4.51				
28.25	4.88				
30.00	5.07		0	5.03	
			.50	5.03	
50.00	6.78		0	5.85	
			1.50	5.85	
			3.00	5.72	
			4.76	4.97	
			6.00	3.43	
			6.75	.82	
			6.78	0	
70.00	7.87		0	6.32	
			3.00	6.32	
			5.50	6.32	
			6.50	6.23	
			7.50	5.62	
			7.80	---	1.41
			8.00	4.68	.39
			8.05	0	
			8.17	1.25	
			8.23	2.50	
80.00	8.20	14.53	0	6.52	
		14.17	2.00	---	
		13.18	4.00	6.52	
		11.21	6.00	---	
		9.54	7.00	6.52	
		8.39	7.50	---	
		7.70	7.75	6.48	
		6.40	8.00	6.39	
			8.25	---	0.80
			8.50	6.09	
			8.84	3.46	
			8.75	2.03	
			8.40	0	
83.00	8.27		0	15.15	
			1.50	14.98	
			2.50	14.68	
			3.50	14.24	
			4.50	13.60	
			5.00	13.19	
			6.00	12.17	
			7.00	10.80	
			8.00	8.80	2.25
			8.25	---	1.45
			8.50	7.25	.45
			9.00	3.65	
			8.75	.92	
			8.57	0	
102.00	8.50		0	15.90	
			2.00	15.62	
			4.00	14.76	
			6.00	13.12	
			7.00	11.84	
			8.00	10.10	
			8.25	---	2.44
			8.50	8.90	1.73
			8.75	---	.88
			9.00	7.20	
			9.35	3.70	
			9.00	.15	
			8.97	0	

Station	Dimensions				
	r	W	X	Y	Z
111.31	8.45		0	15.90	
			2.00	15.62	
			4.00	14.76	
			6.00	13.12	
			7.00	11.63	
			7.50	10.67	3.93
			7.75	---	3.45
			8.00	9.35	---
			8.25	---	2.20
			8.50	7.58	1.35
			8.95	2.85	---
			8.75	0	---
120.88	8.28		0	15.90	
			2.00	15.62	
			4.00	14.76	
			6.00	12.91	
			7.00	10.61	
			7.38	8.10	
			7.66	6.00	3.50
			8.00	3.98	2.18
			8.15	---	1.57
			8.25	2.18	1.15
			8.40	.33	
			8.39	0	
130.00	8.02		0	15.90	
			2.00	15.62	
			4.00	14.76	
			5.80	12.98	
			6.25	10.50	
			6.30	7.30	
			6.50	5.40	
			7.00	4.03	
			7.50	---	2.82
			7.75	2.20	2.07
			8.00	.95	.79
			8.05	0	
134.00	7.82	15.90	0	6.85	
		15.62	2.00	6.59	
		14.76	4.00	6.11	
		13.76	5.25	---	
		13.18	5.60	5.96	
		12.81	5.70	5.98	
		12.00	5.80	---	
		6.70	5.80	5.96	
		6.00	5.85	---	
		5.28	6.00	---	
			5.00	5.90	
			5.50	5.90	
140.00	7.60		0	7.40	
			1.92	7.16	
			3.74	6.46	
			4.28	6.12	
			4.88	5.82	
			5.37	5.37	
145.00	7.34				

Note: See figure 11(c) for definition of symbols.
See table IV for radii of nose and tail portions of fuselage.

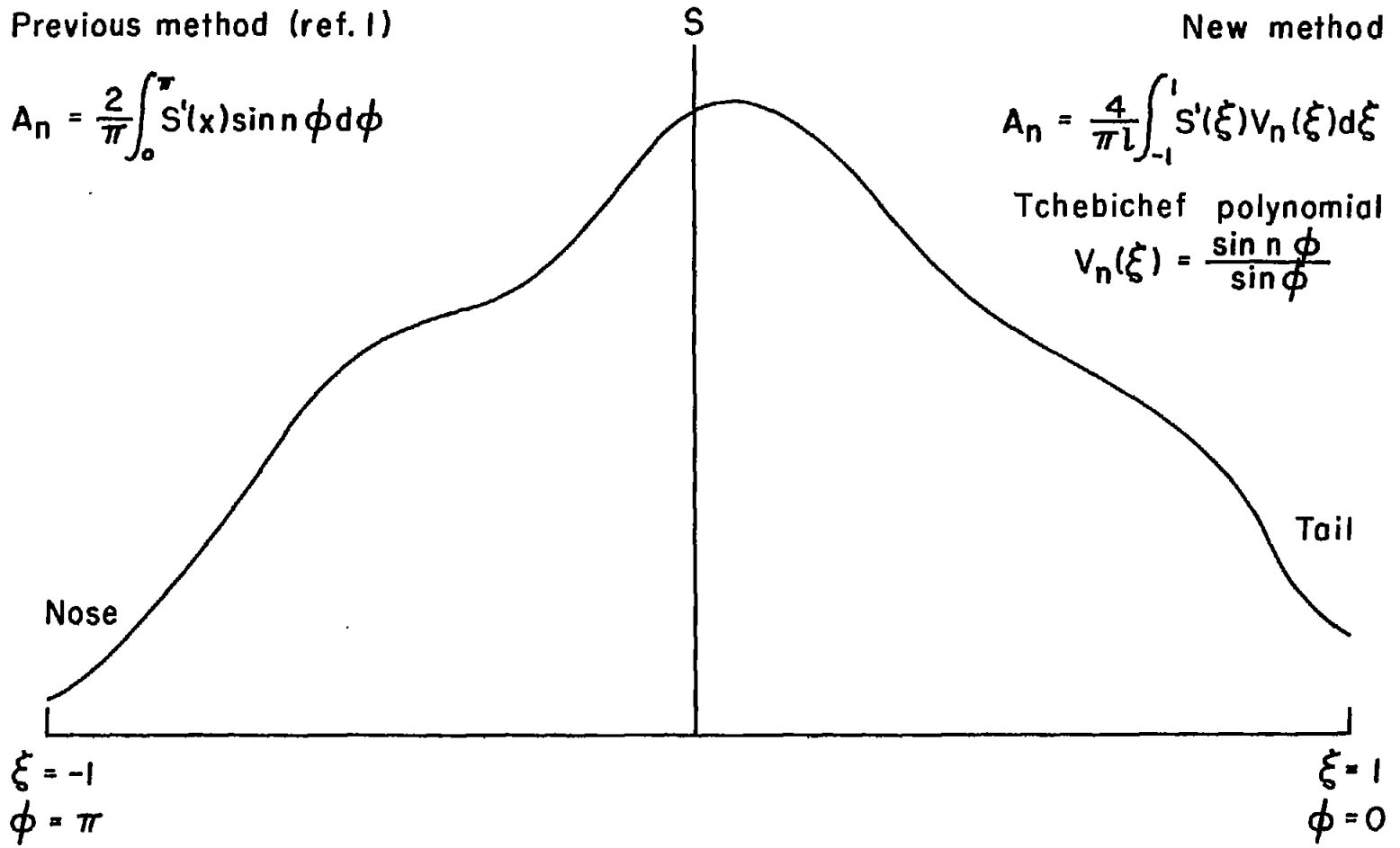

Figure 1.- Definition of the Tchebichef polynomials used to represent the Fourier sine series defining the slope of the area distribution curves of a model.

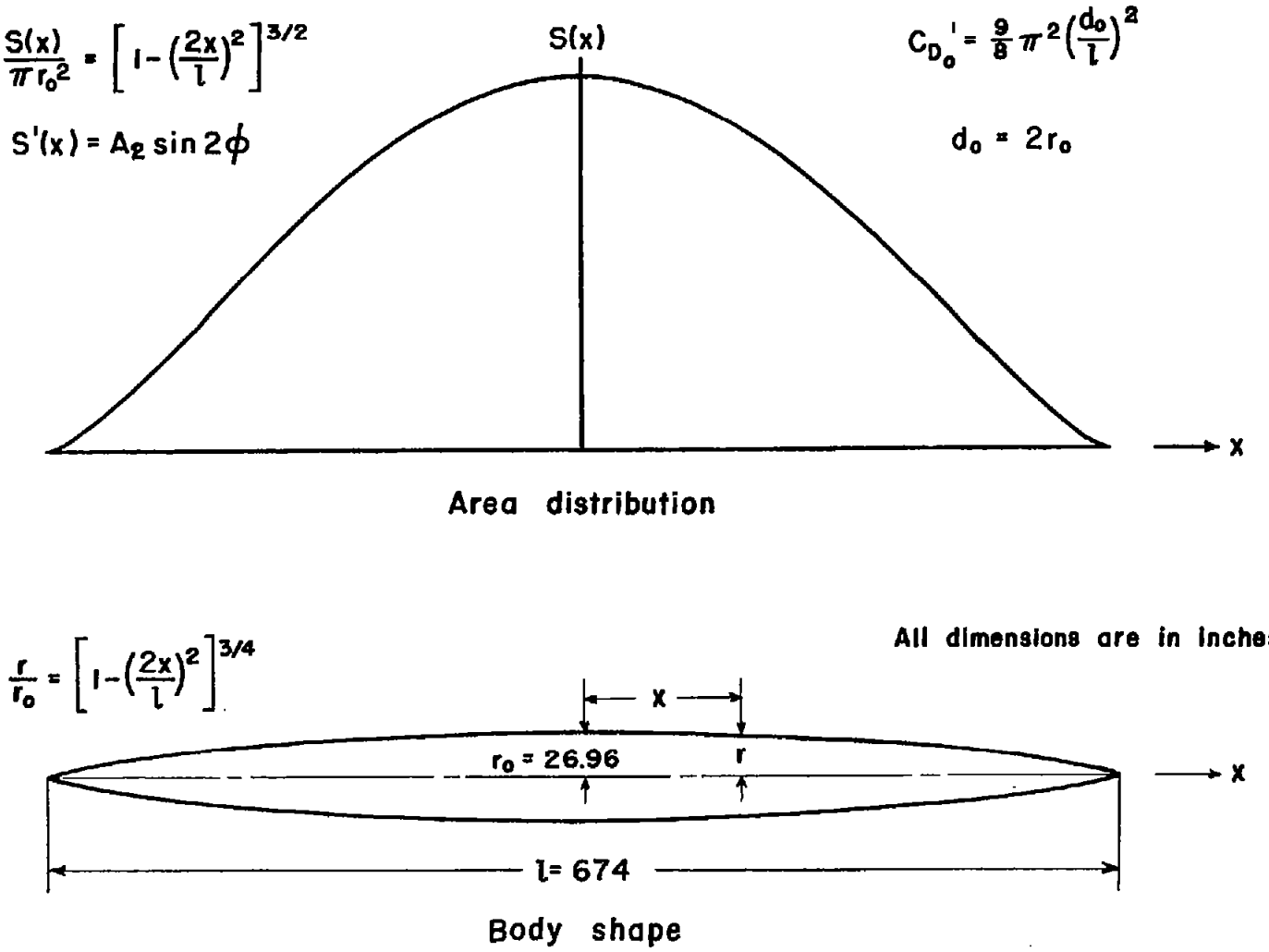

Figure 2.- Minimum-drag body for prescribed volume and length (Sears-Haack body); fineness ratio 12.5.

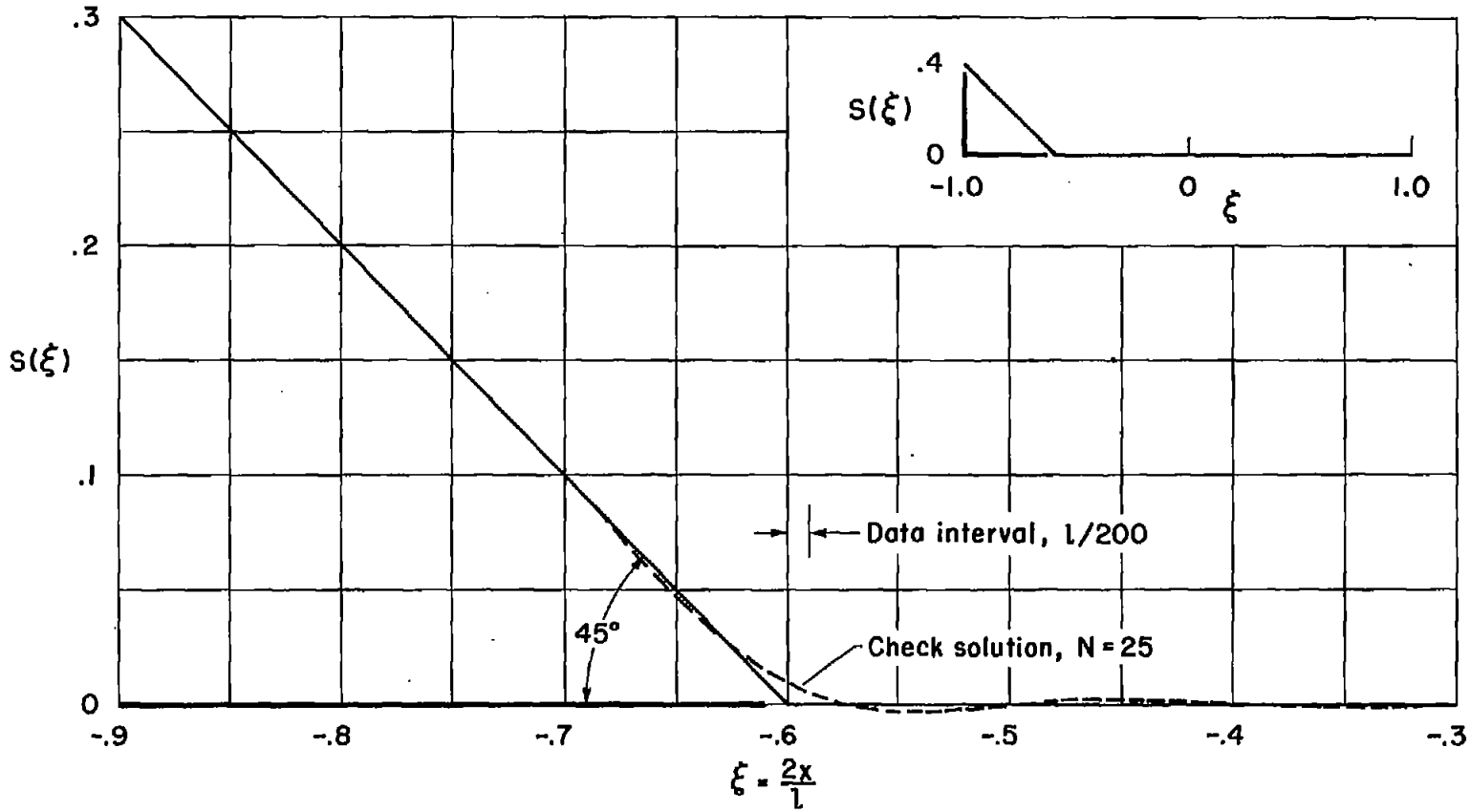

(a) An enlarged portion of the area curve, with the Tchebichef check solution for N = 25.

Figure 3.- Simplified area curve with a discontinuity of slope.

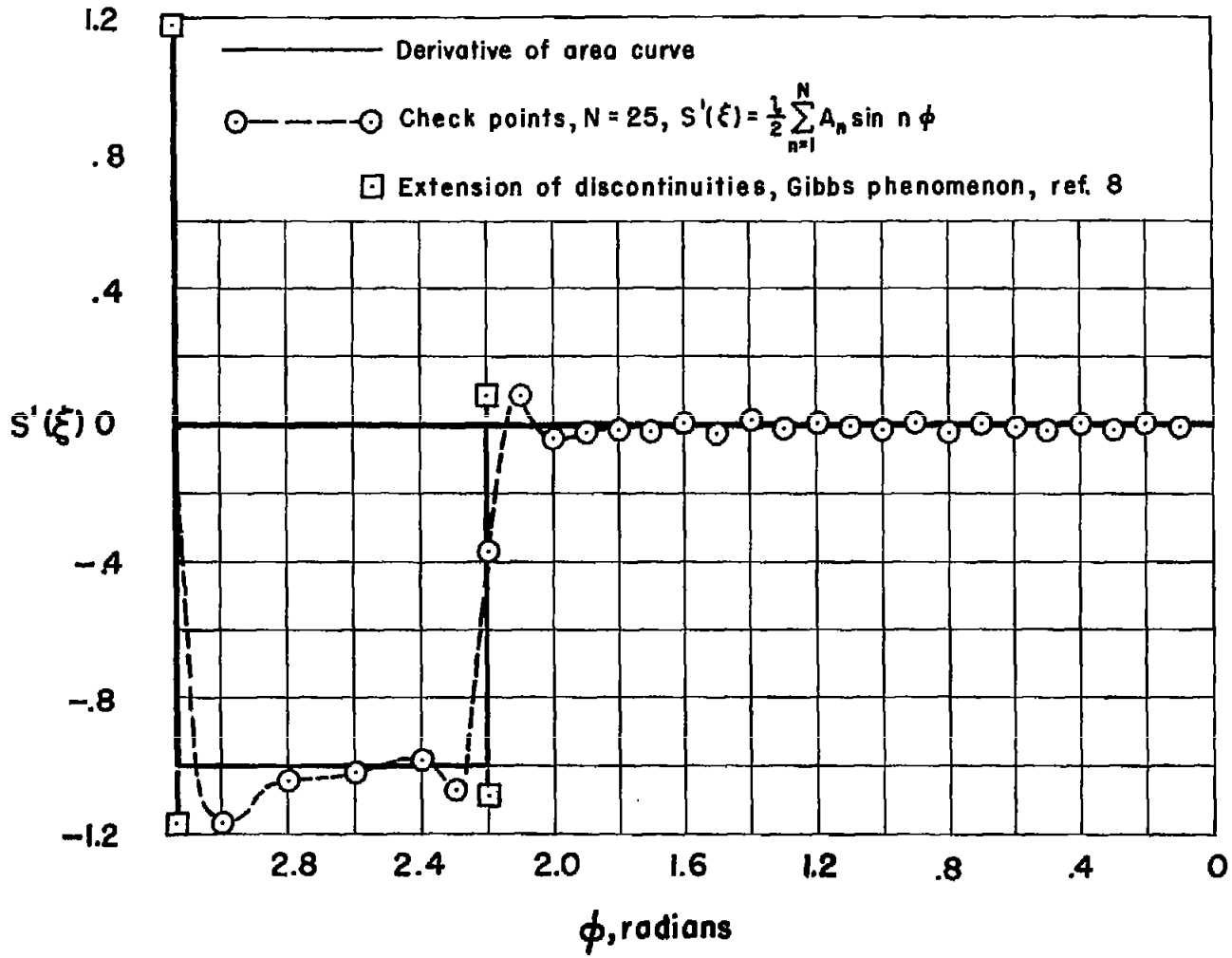

(b) Derivative of area curve and check points for N = 25.

Figure 3.- Concluded.

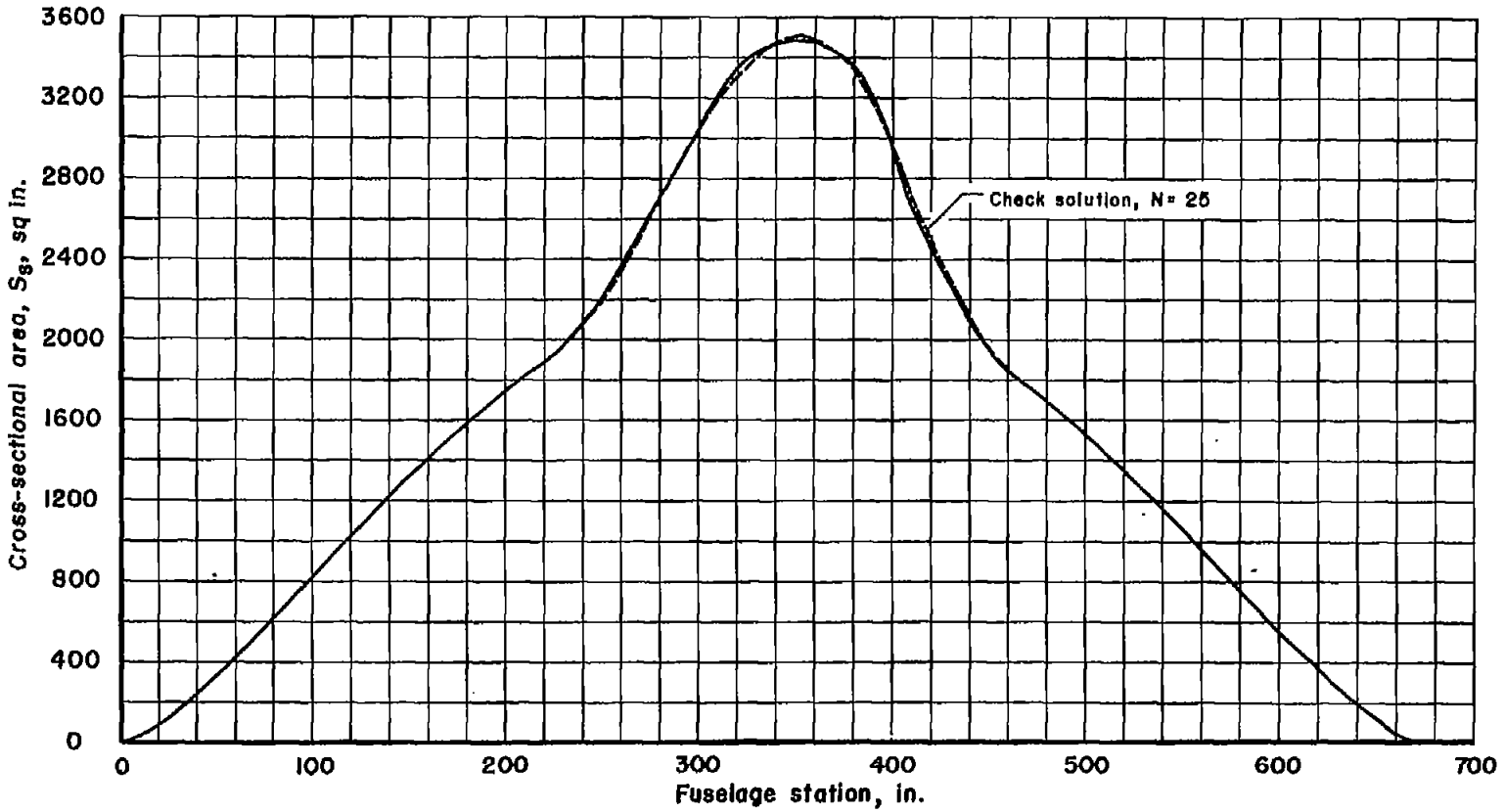

(a) No discontinuity of slope, M = 1.5, $\theta = 90^\circ$, $\psi = 0^\circ$.

Figure 4.- Plot of Tchebichef check solutions for area curves previously analyzed (ref. 3).

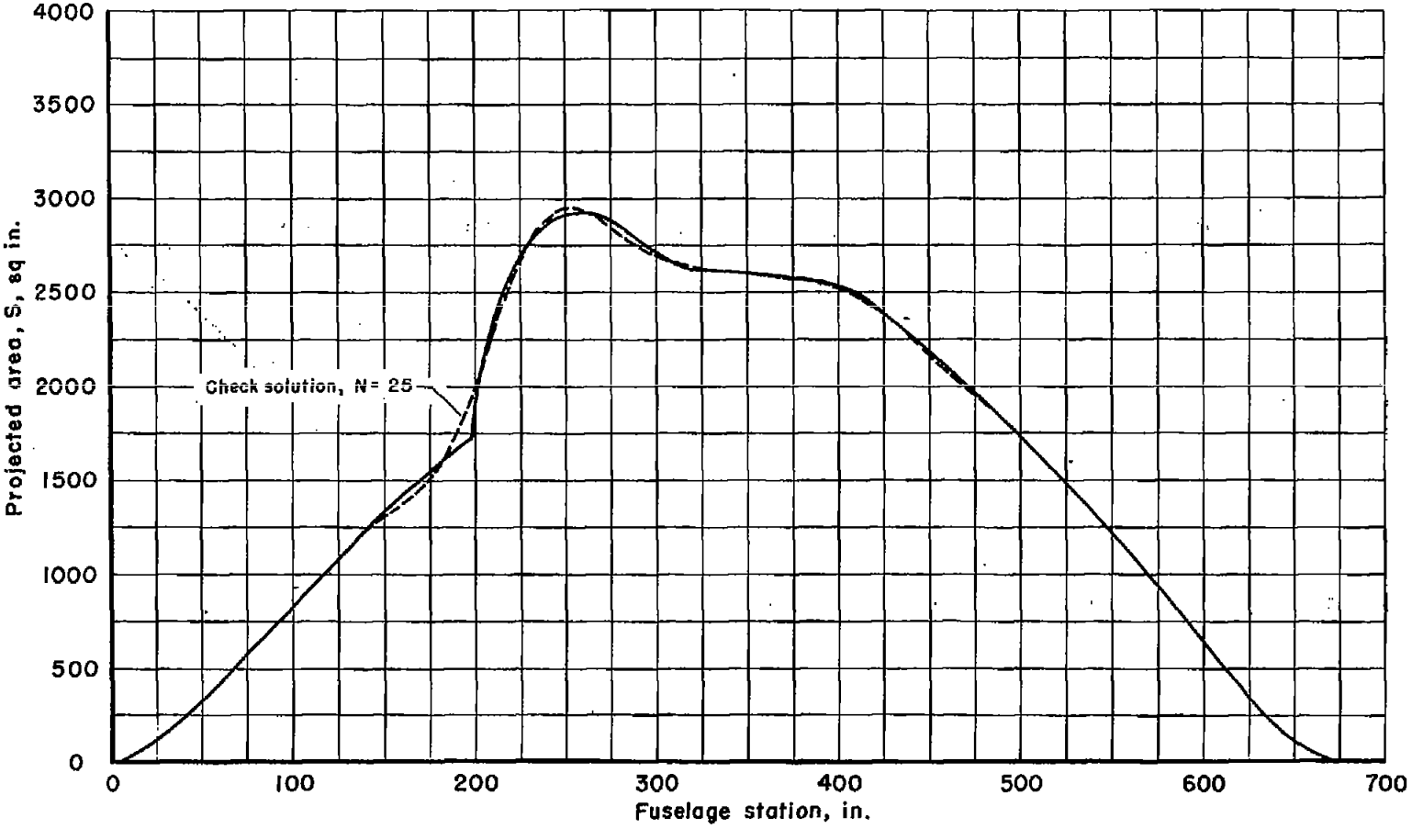

(b) Discontinuity of slope, M = 1.5, θ = 22.5°, ψ = 46.0°.

Figure 4.- Concluded.

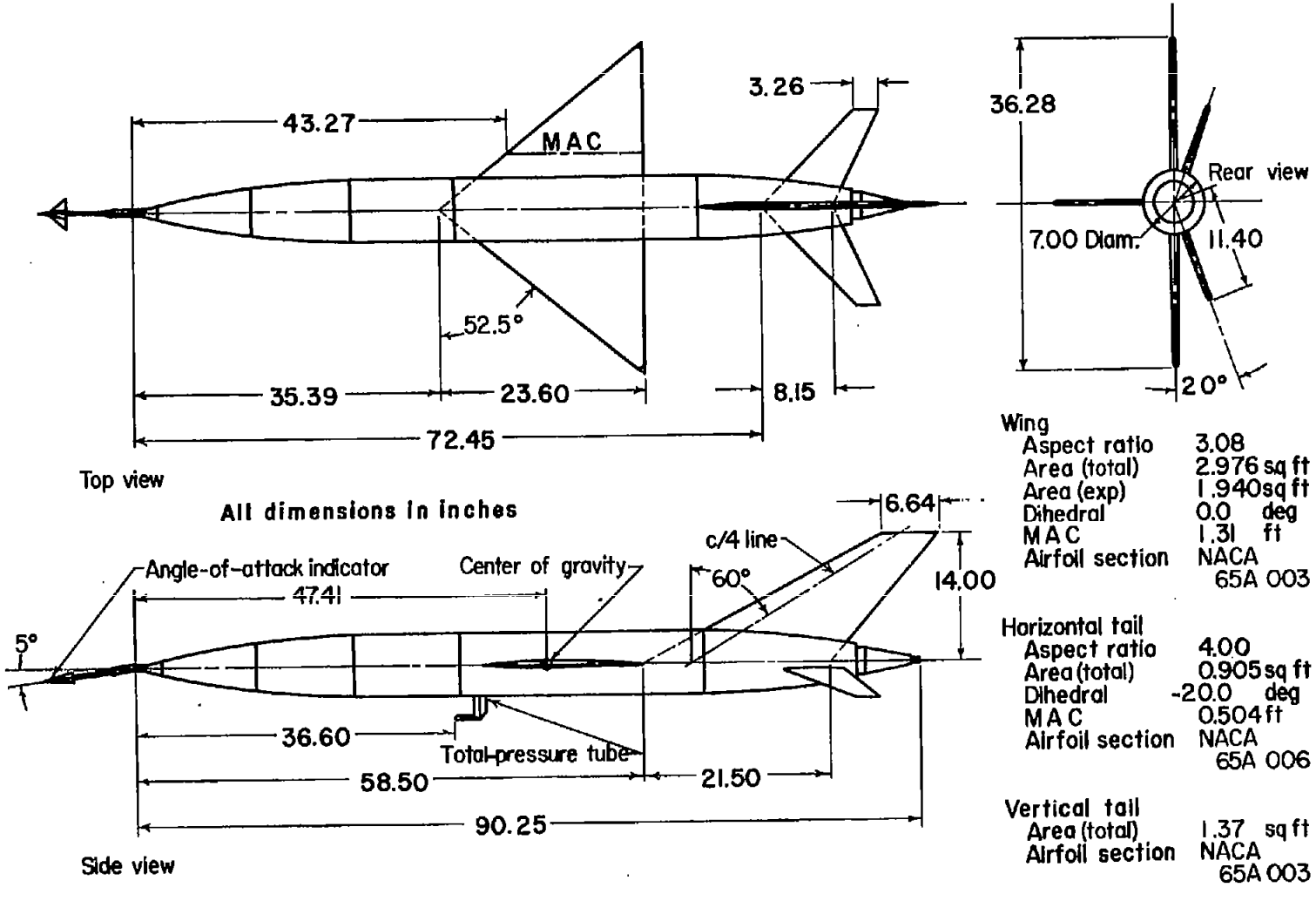

Figure 5.- Triangular-wing interceptor-type airplane model (ref. 9); Model 1.

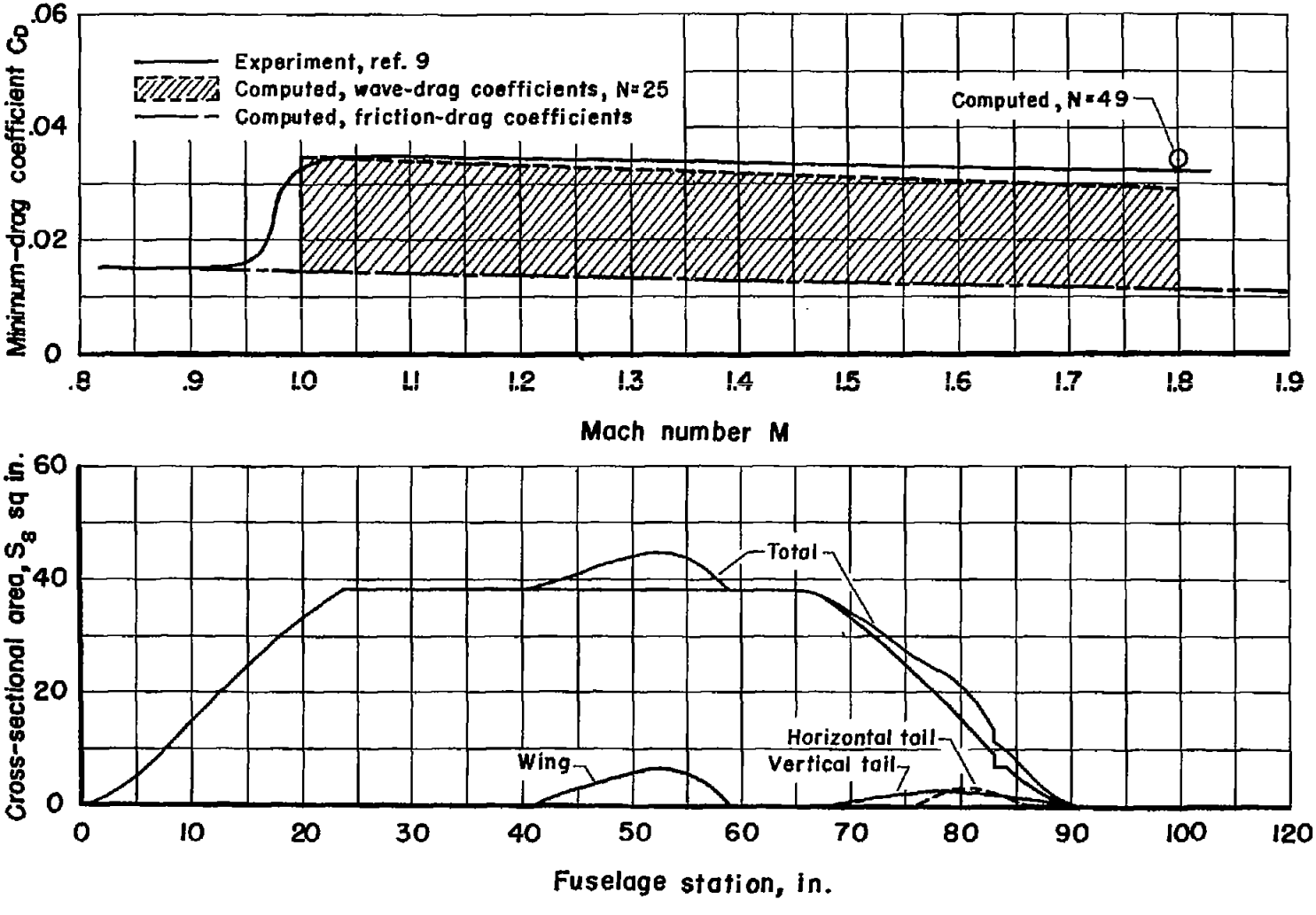

Figure 6.- Triangular-wing airplane (Model 1, fig. 5) minimum-drag coefficients and cross-sectional area distribution.

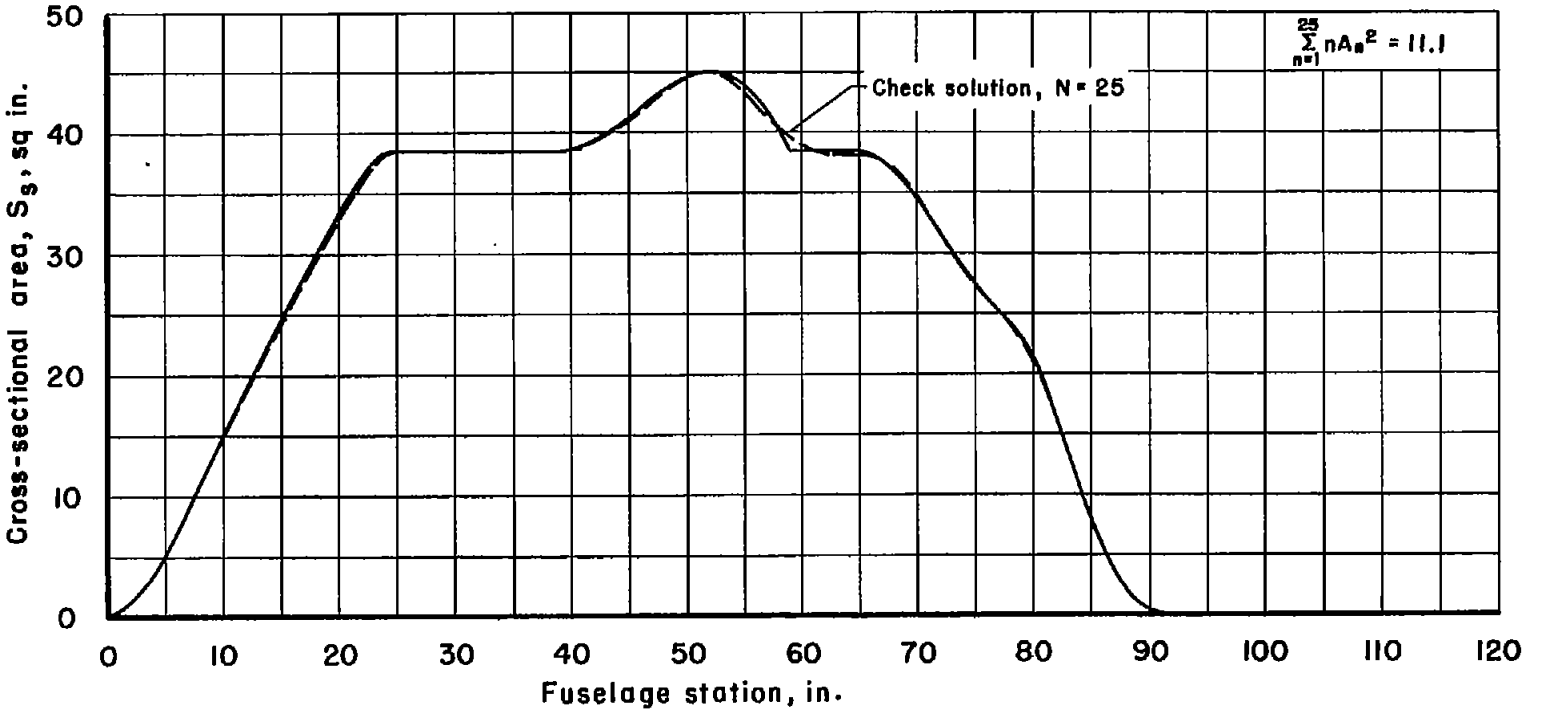

(a) M = 1.00

Figure 7.- Projected-area distribution for the triangular-wing airplane (Model 1) for Mach numbers of 1.0, 1.2, and 1.8 with check solutions for N = 25.

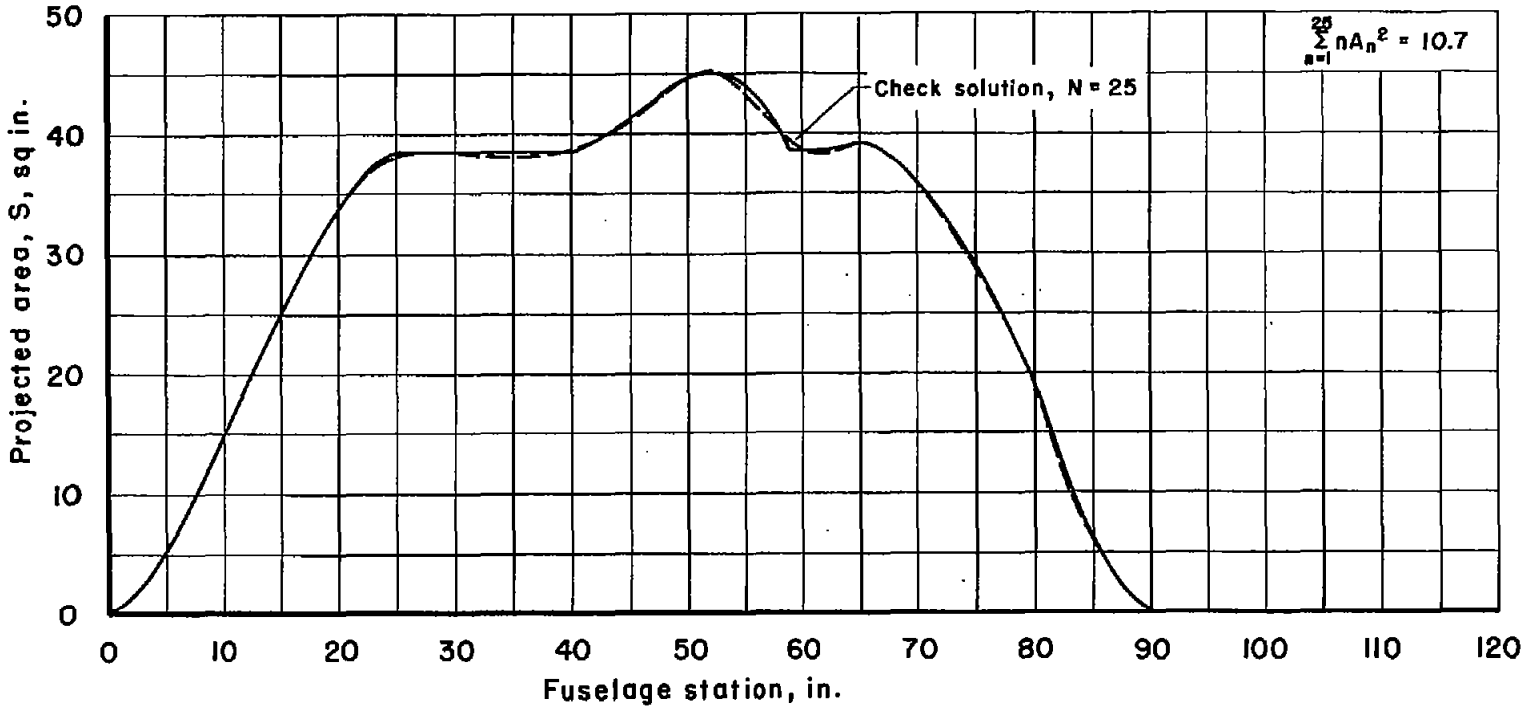

(b) M = 1.2, $\theta = 90^\circ$, $\psi = 0^\circ$

Figure 7.- Continued.

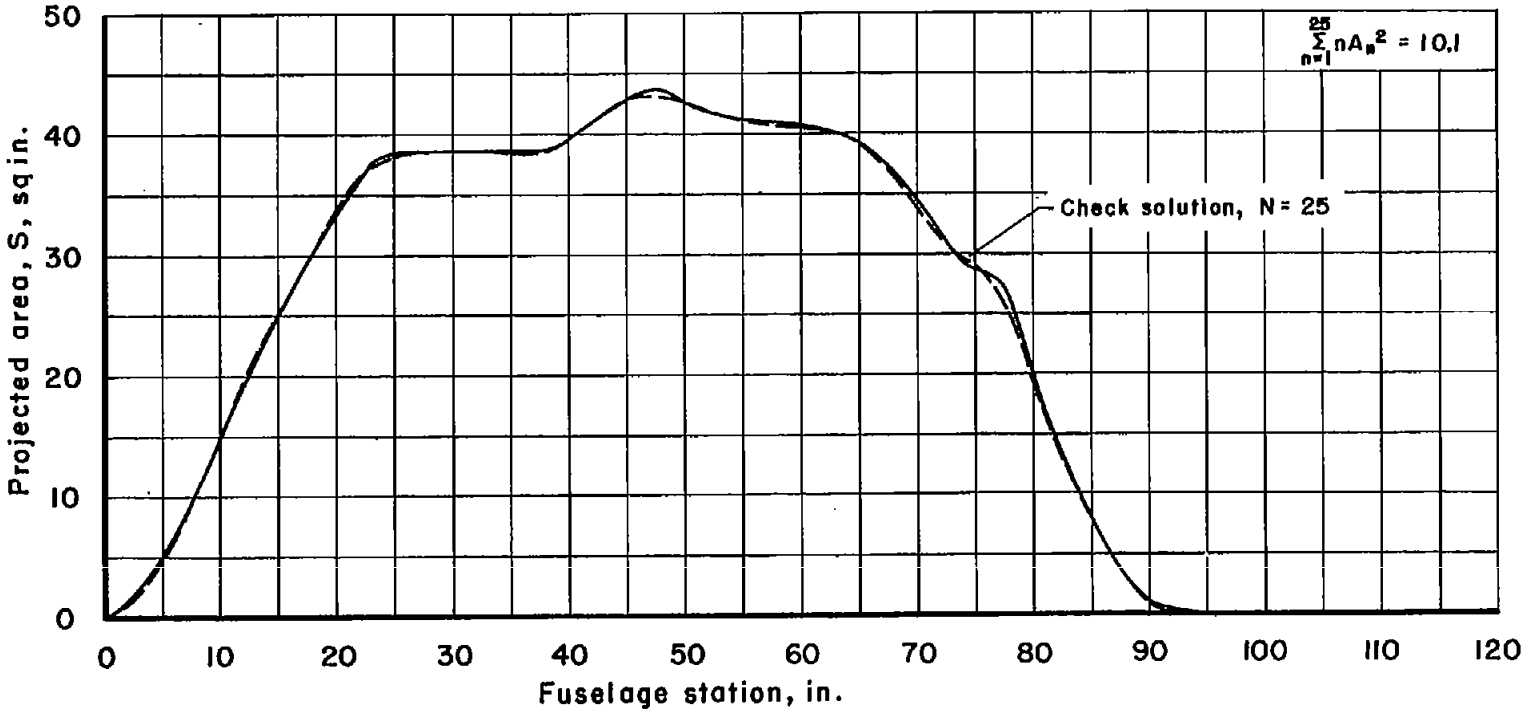

(c) M = 1.2, $\theta = 180^\circ$, $\psi = 33.6^\circ$

Figure 7.- Continued.

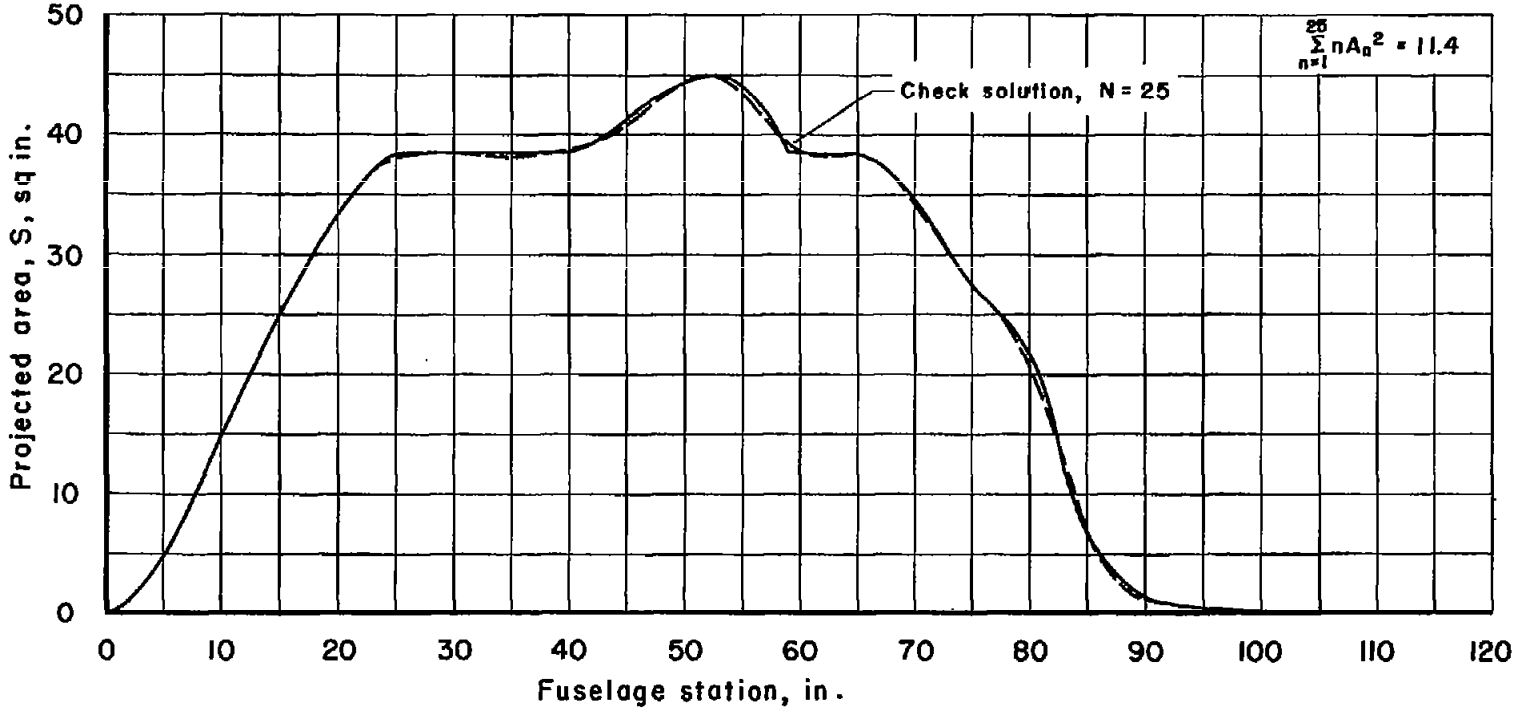

(d) M = 1.2, $\theta = 270^\circ$, $\psi = 0^\circ$

Figure 7.- Continued.

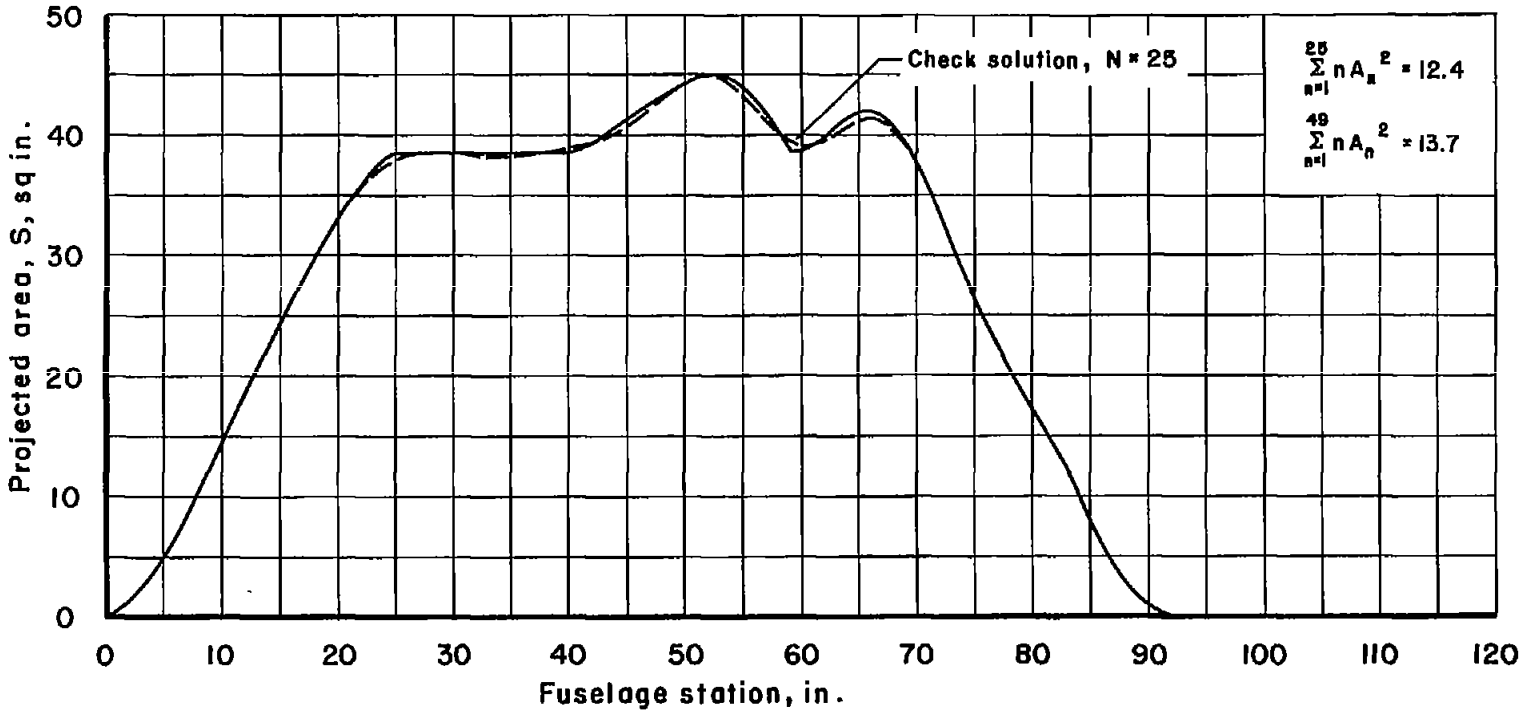

(e) M = 1.8, $\theta = 90^\circ$, $\psi = 0^\circ$

Figure 7.- Continued.

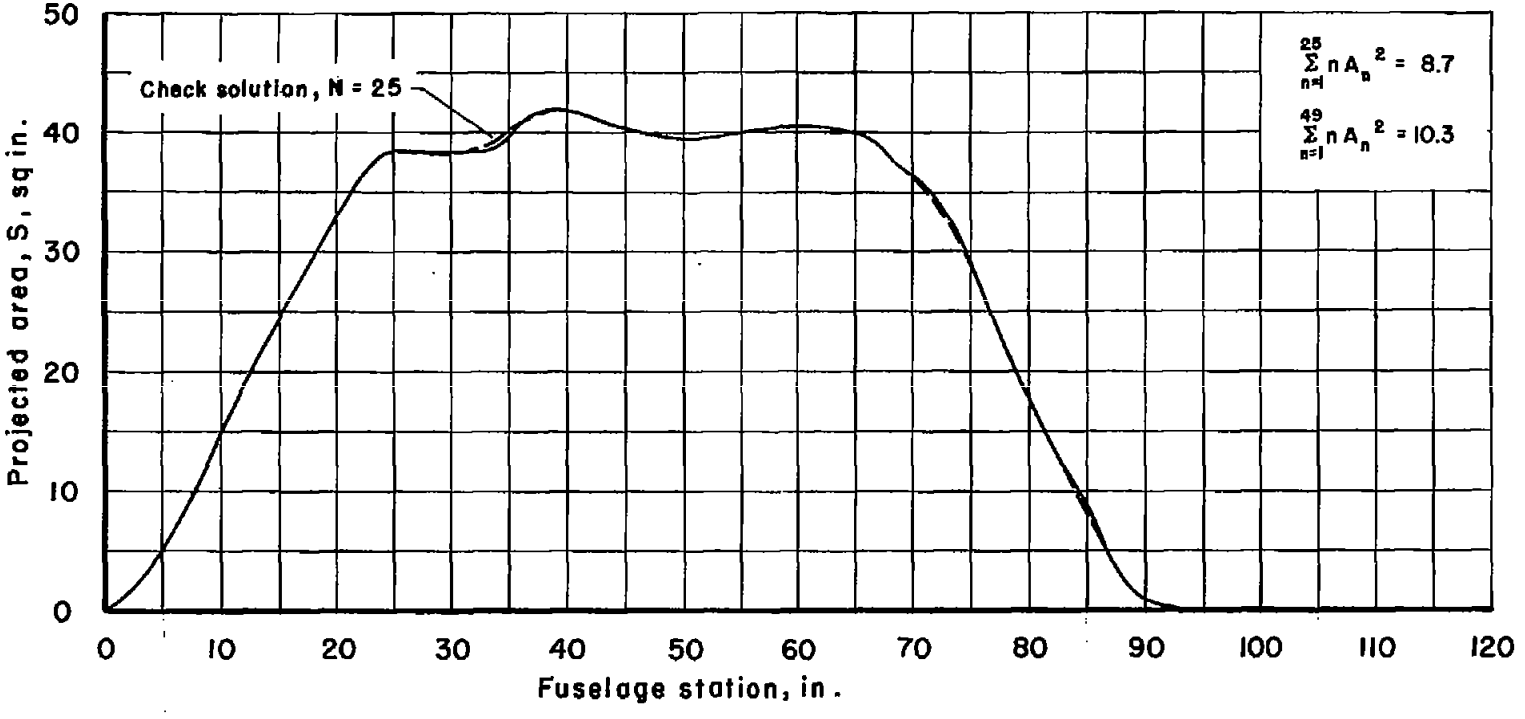

(f) M = 1.8, $\theta = 180^\circ$, $\psi = 56.3^\circ$

Figure 7.- Continued.

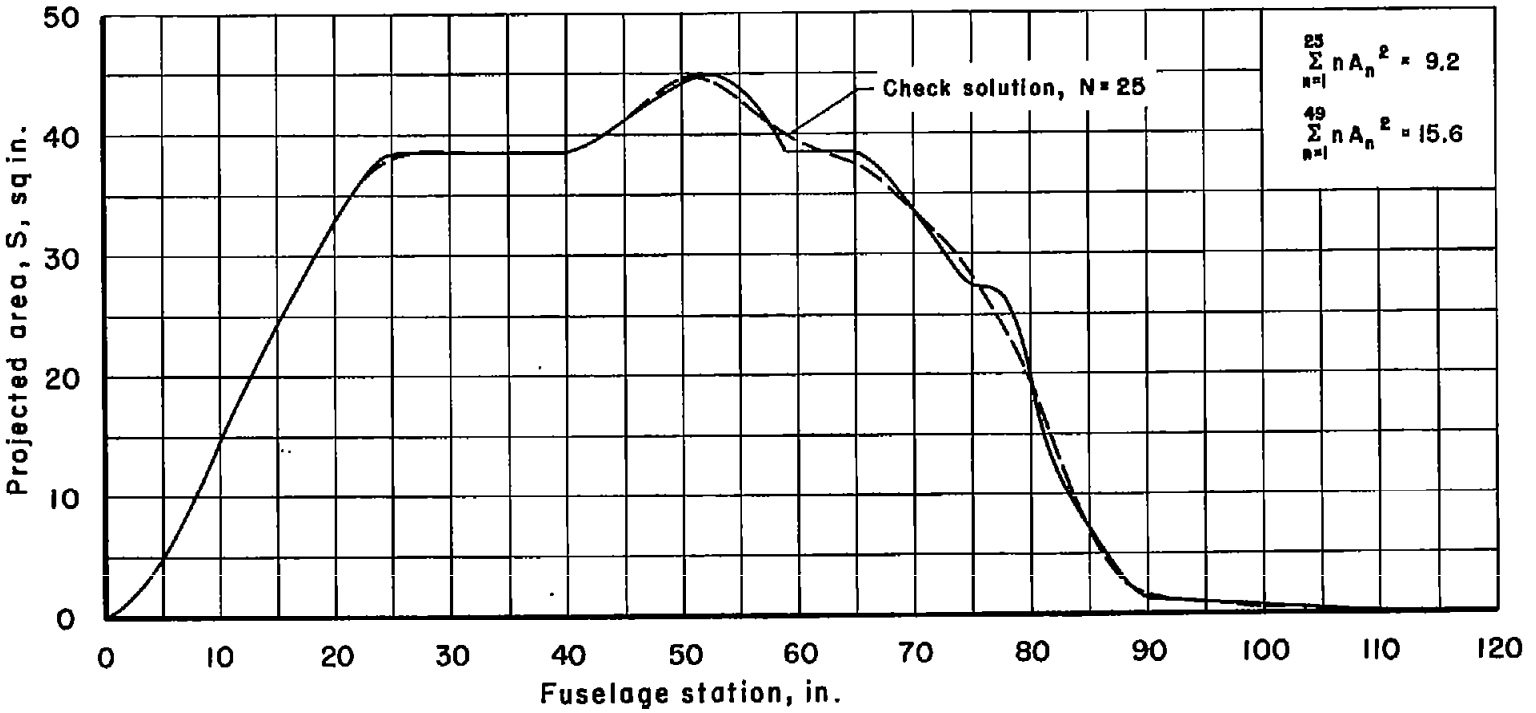

(g) M = 1.8, $\theta = 270^\circ$, $\psi = 0^\circ$

Figure 7.- Concluded.

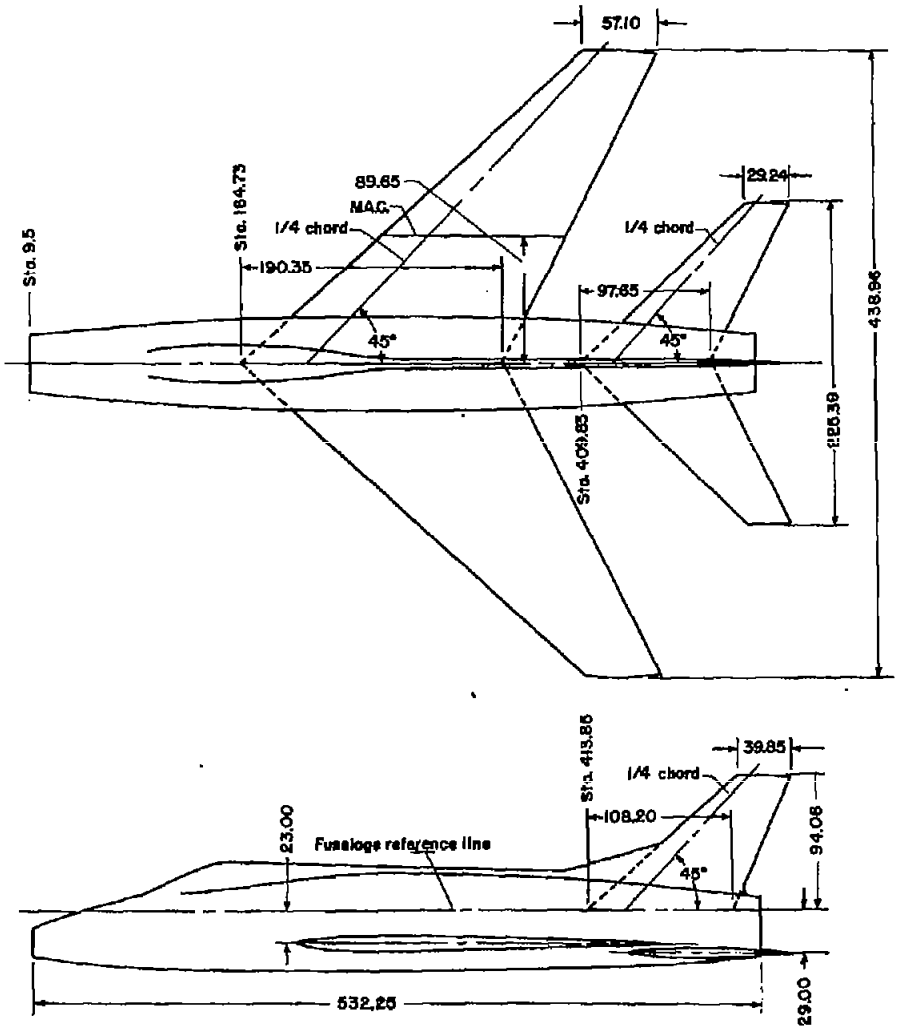

WING
- Aspect ratio, 3.56
- Area (total), 376.02 sq ft
- Dihedral angle, 0 deg
- M.A.C. 11.33 ft
- Airfoil section, NACA 64A007

HORIZONTAL TAIL
- Aspect ratio, 3.56
- Area (total), 99.00 sq ft
- Dihedral angle, 0 deg
- M.A.C. 5.81 ft
- Airfoil section, NACA 64A007

VERTICAL TAIL
- Aspect ratio, 1.27
- Area (excluding dorsal fin), 48.35 sq ft
- M.A.C. 6.61 ft
- Airfoil section, NACA 64A007

All dimensions in inches.
All airfoil sections parallel to the fuselage center line.

Figure 8.- Swept-wing interceptor-type airplane similar to low-tail version of reference 11; Model 2.

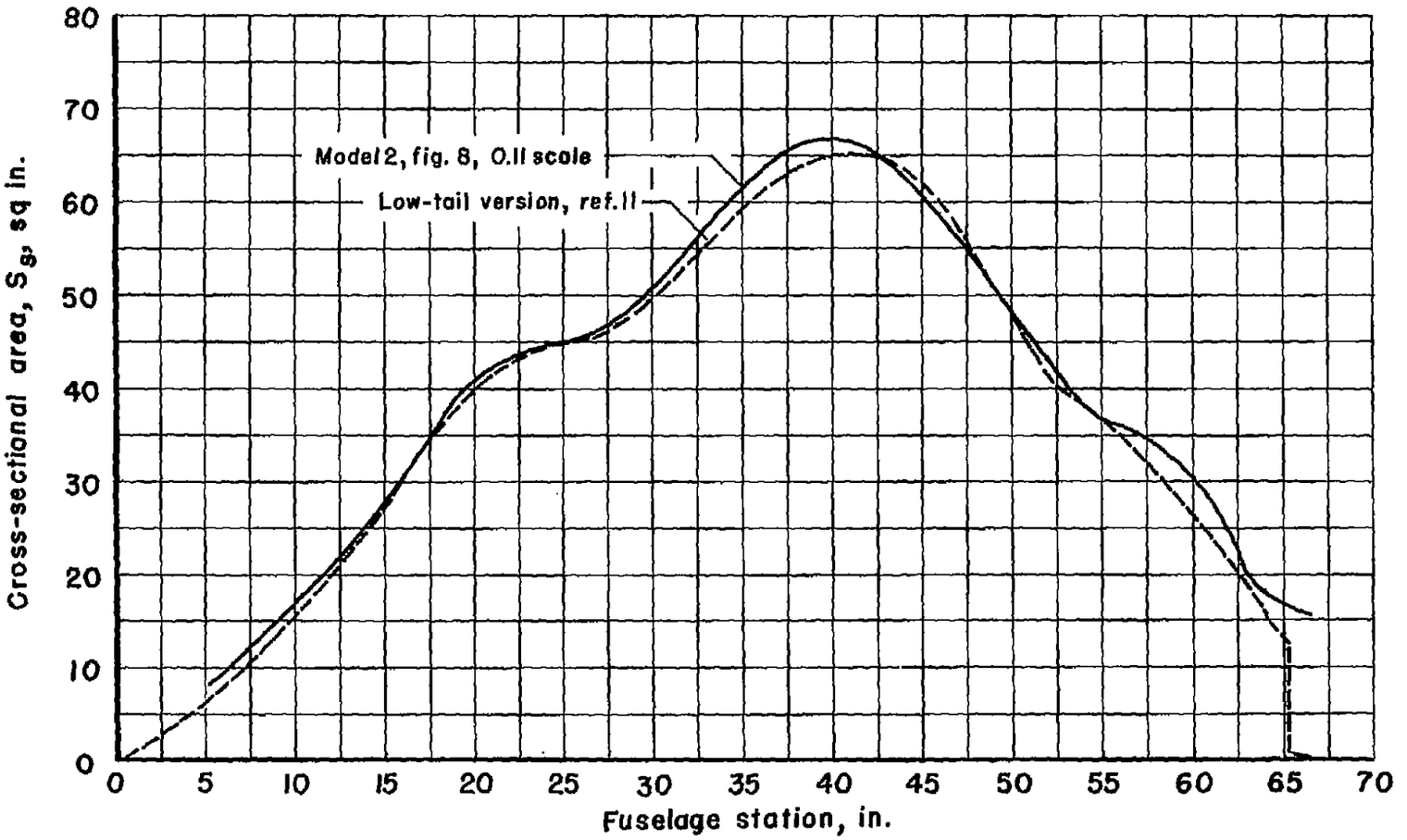

Figure 9.- Cross-sectional area distributions of low-tail versions of a swept-wing airplane (0.11 scale models).

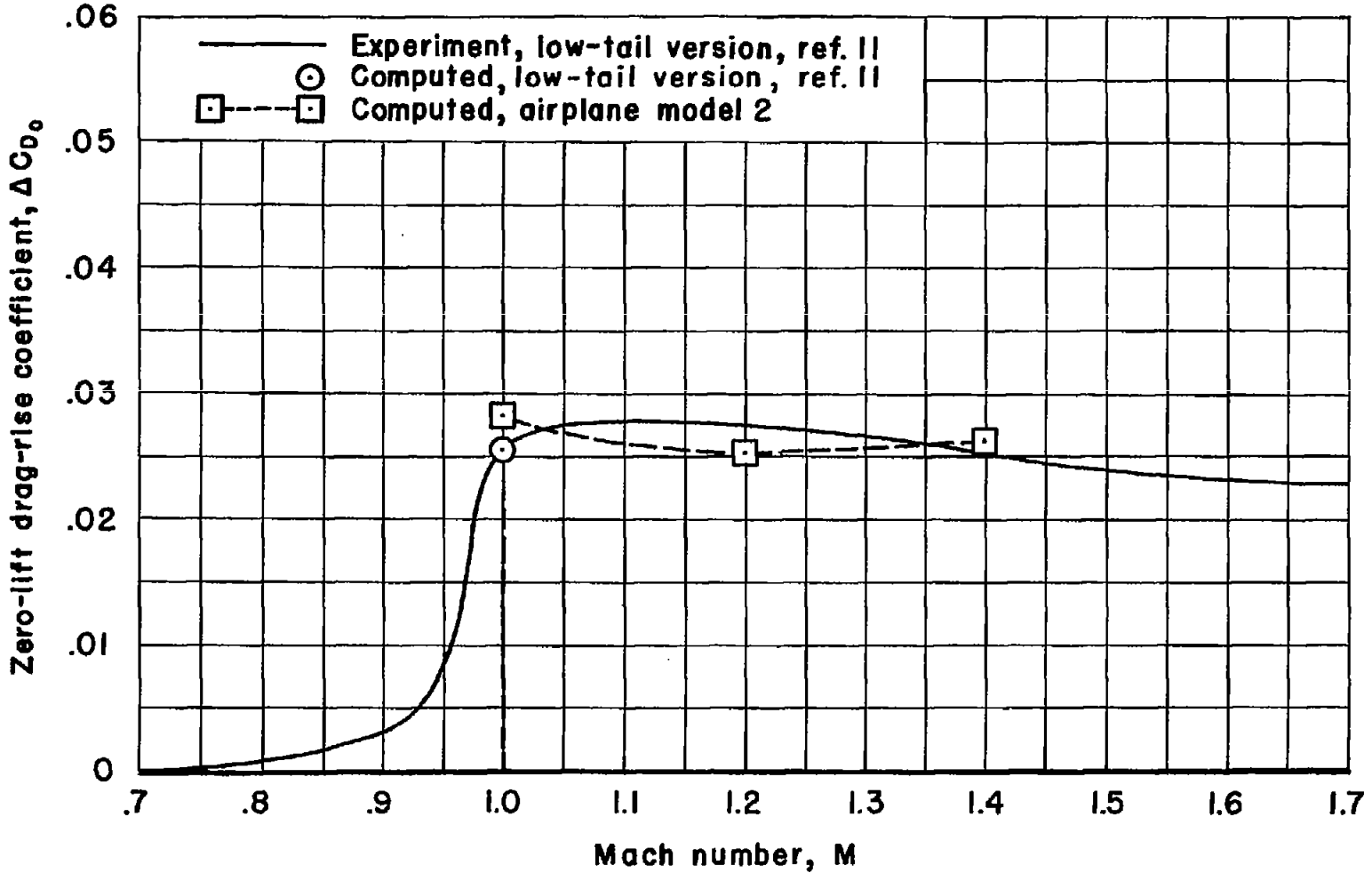

Figure 10.- Comparison of experimental drag-rise coefficients from reference 11 with computed wave-drag coefficients (N = 25) for two low-tailed versions of a swept-wing airplane.

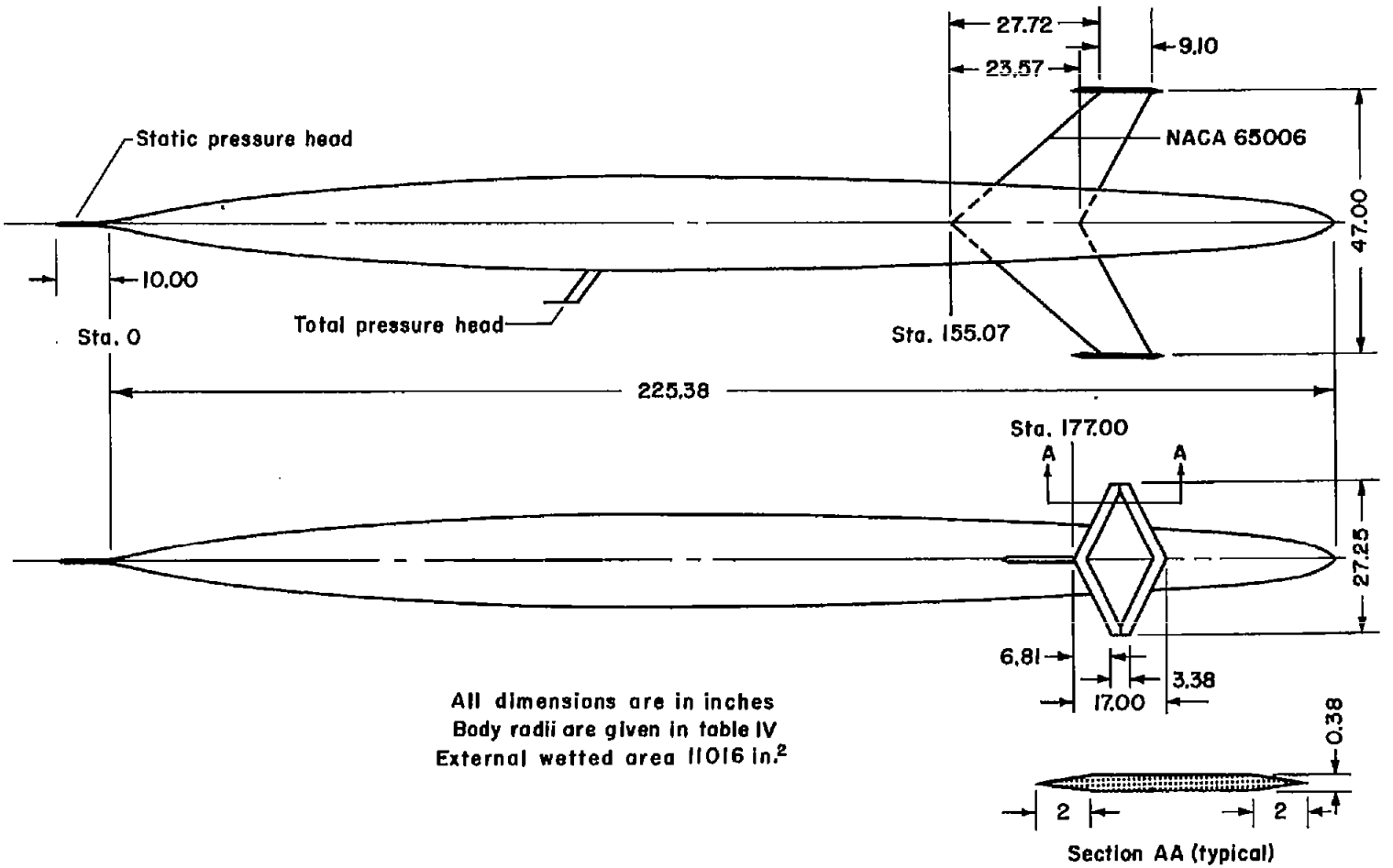

(a) Basic body and tail.

Figure 11.- Scoop-inlet duct model; Model 3.

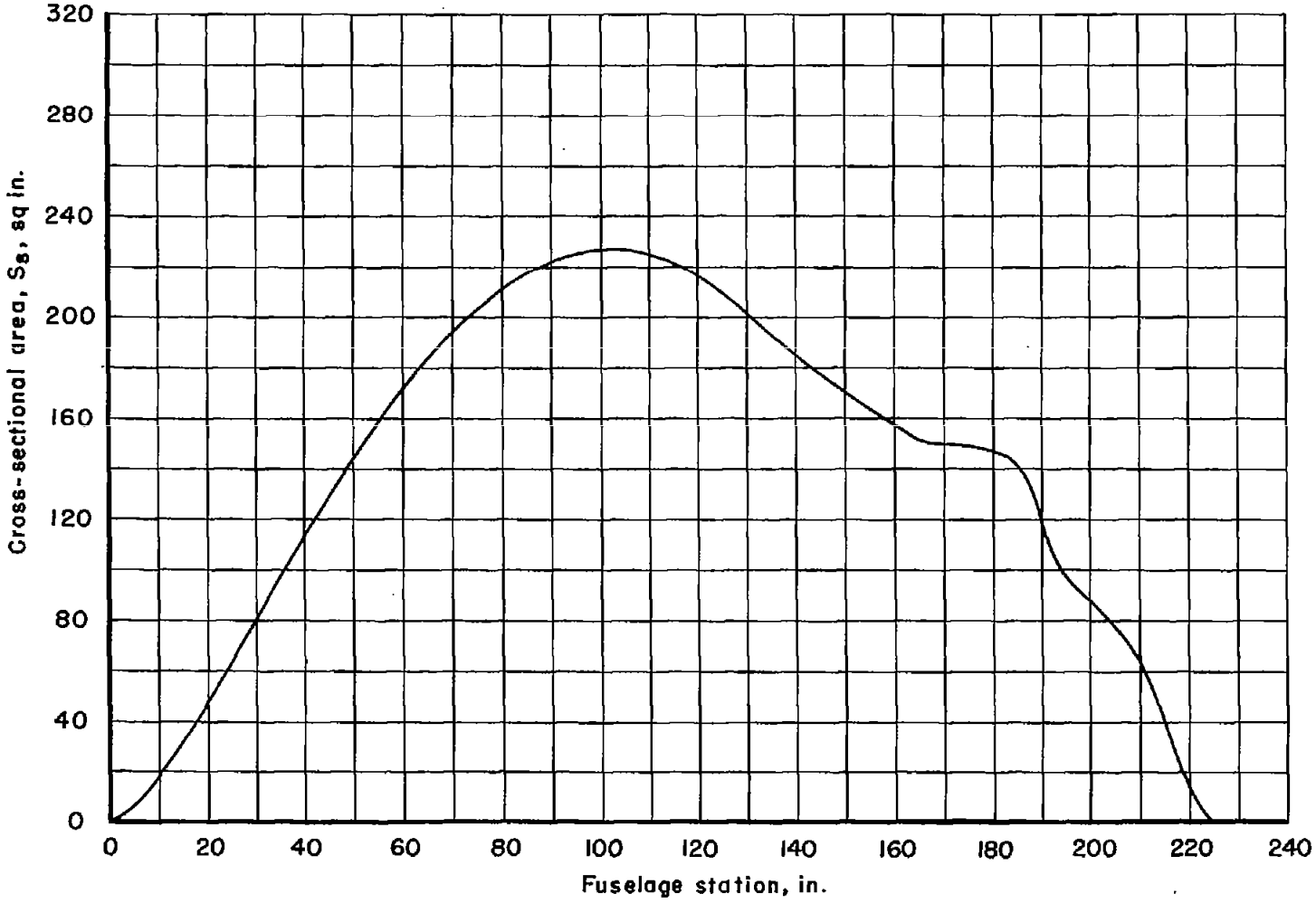

(b) Area distribution of the basic body and tail.

Figure 11.- Continued.

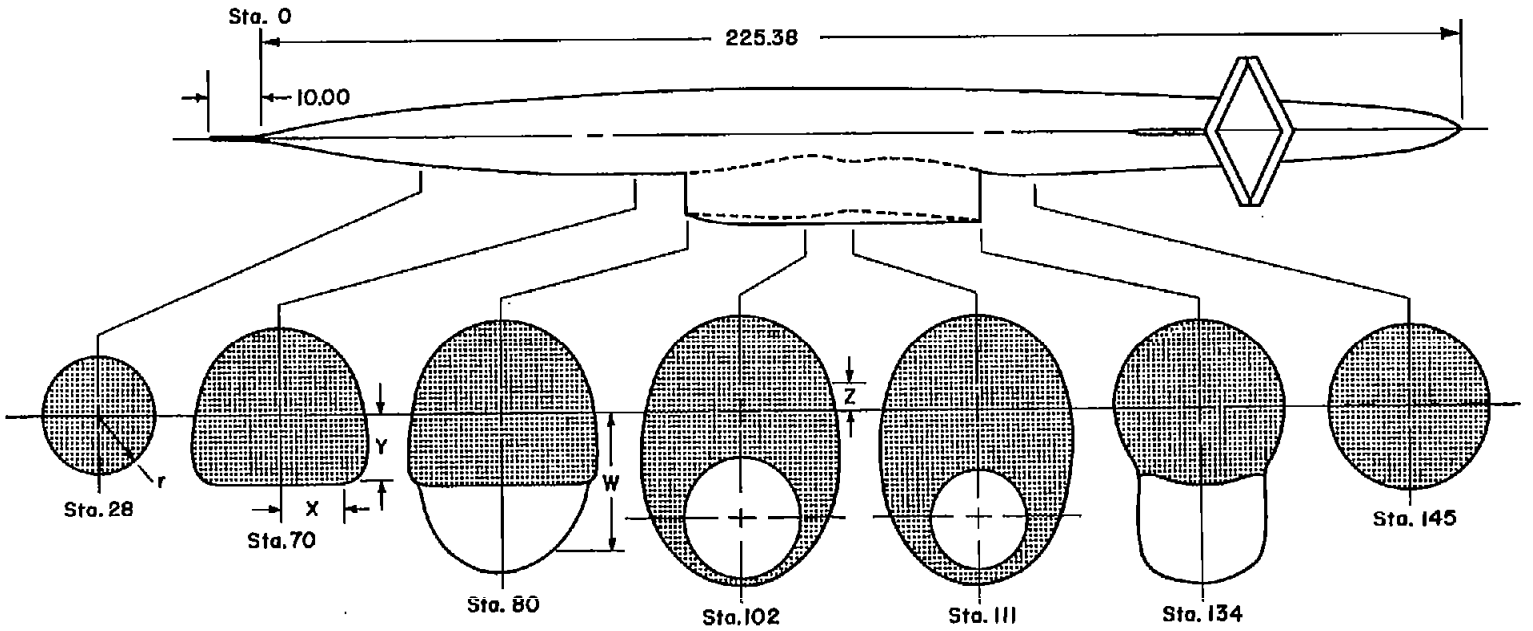

All dimensions are in inches
Dimensions X, Y, W, and Z are given in table V
Body radii are given in table V
External wetted area 11850 in.^{2}

Duct areas:
Entrance; 95.28 in.^{2} (L.E., round lip, Sta. 80)
84.79 in.^{2} (Sta. 81.5)
Entrance to throat; 96.82 in.^{2} (Sta. 102.5)
Outlet; 99.55 in.^{2} (Sta. 134)

(c) Scoop inlet and duct.

Figure 11.- Concluded.

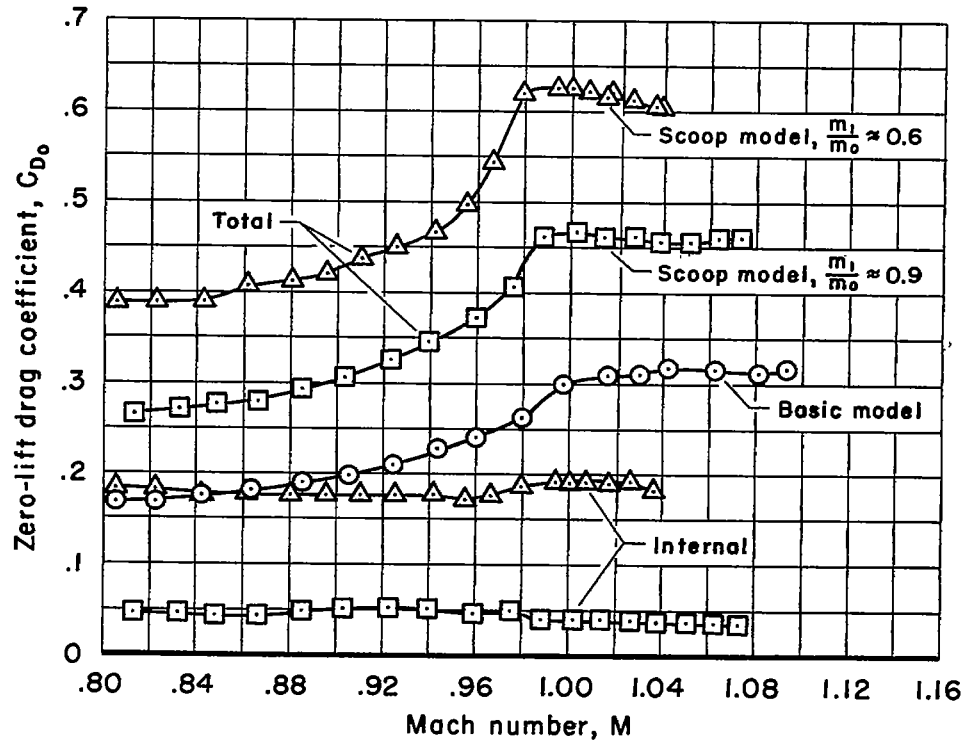

(a) Total and internal drag coefficient.

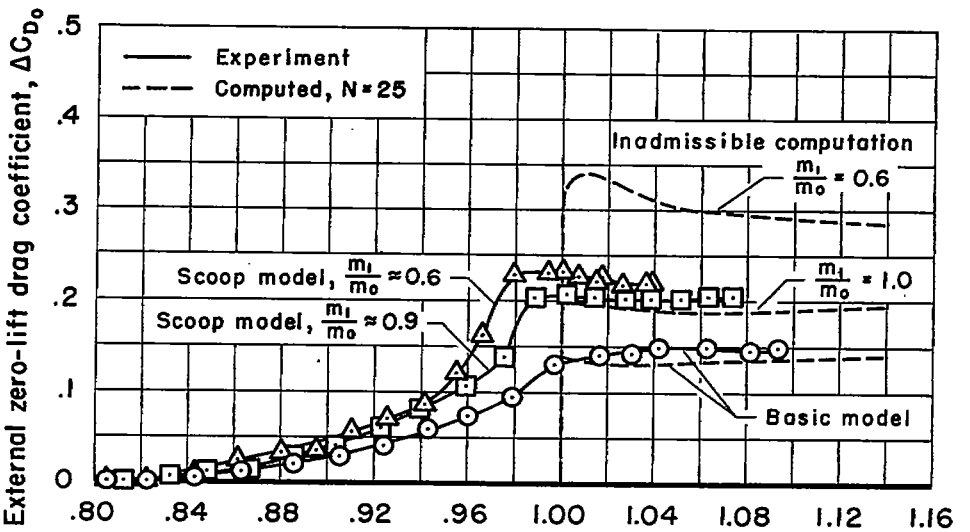

(b) External drag-rise coefficient.

Figure 12.- Experimental and computed drag coefficients for the scoop-inlet-duct model; Model 3.

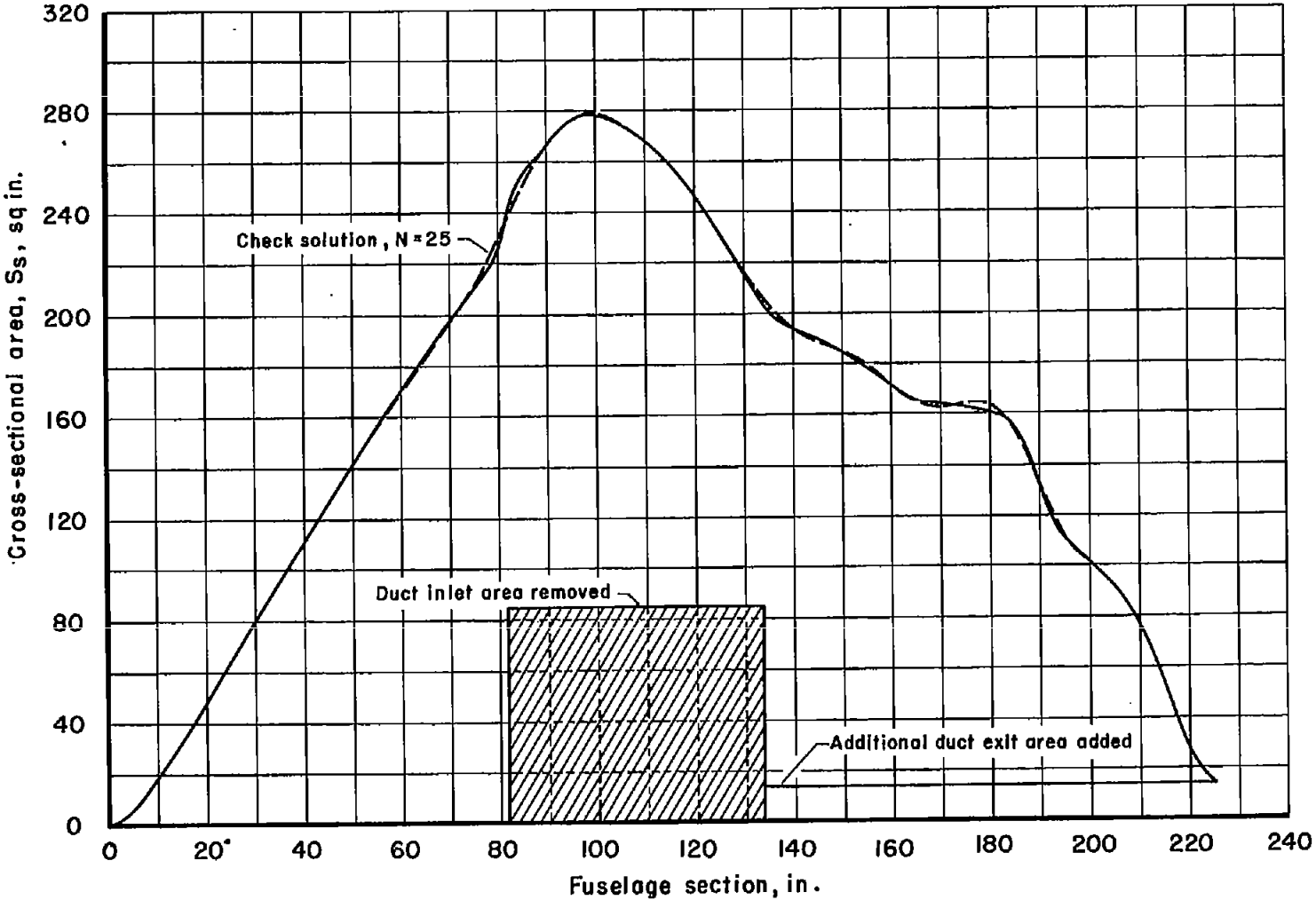

Figure 13.- Equivalent cross-sectional area distribution of the scoop-inlet-duct model for a duct-air mass-flow ratio of 1.0.

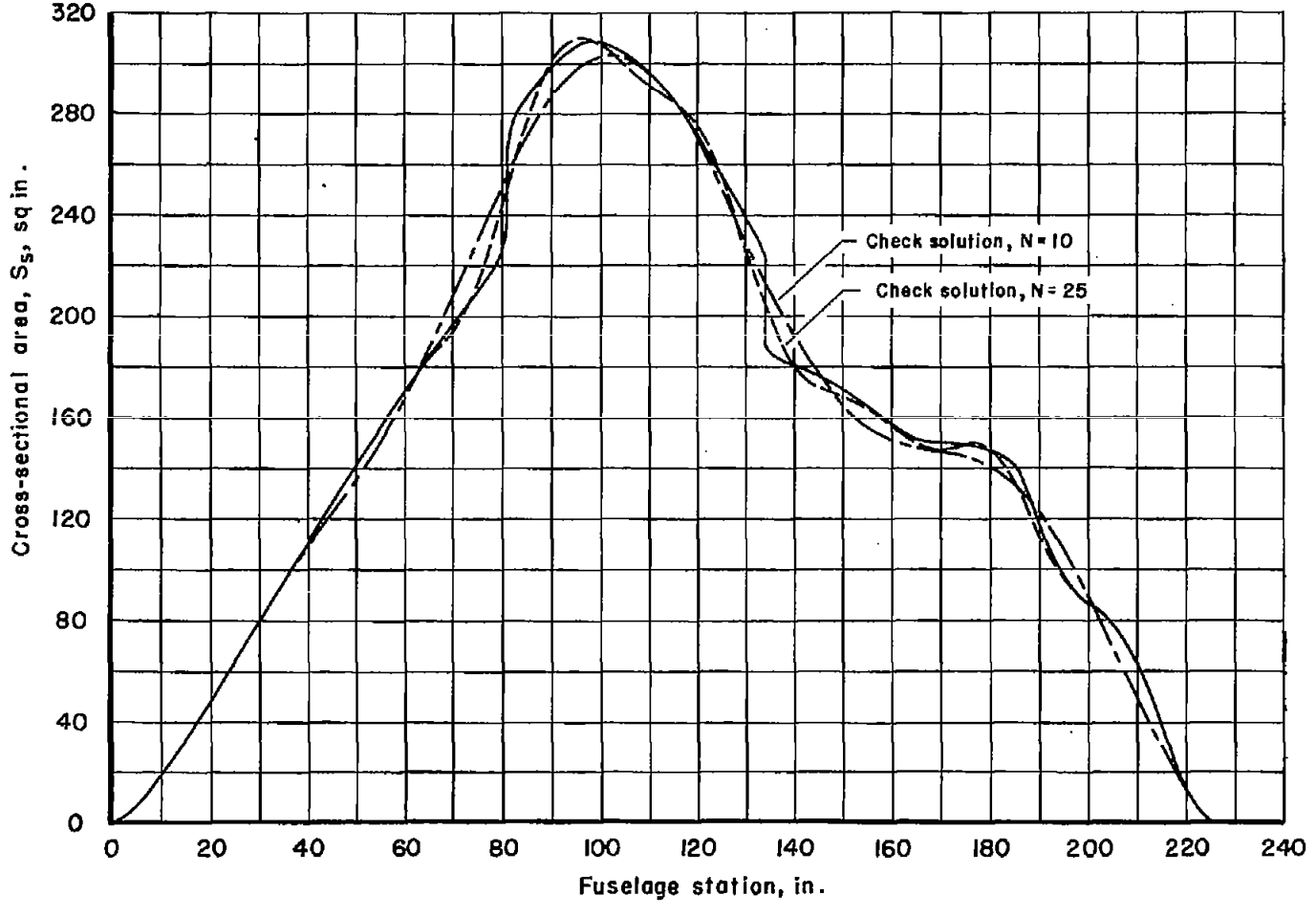

(a) Inadmissible check solutions for N = 10 and N = 25.

Figure 14.- An inadmissible area curve with infinite slopes. Scoop-inlet duct model for duct mass-flow ratio of 0.6; Model 3.

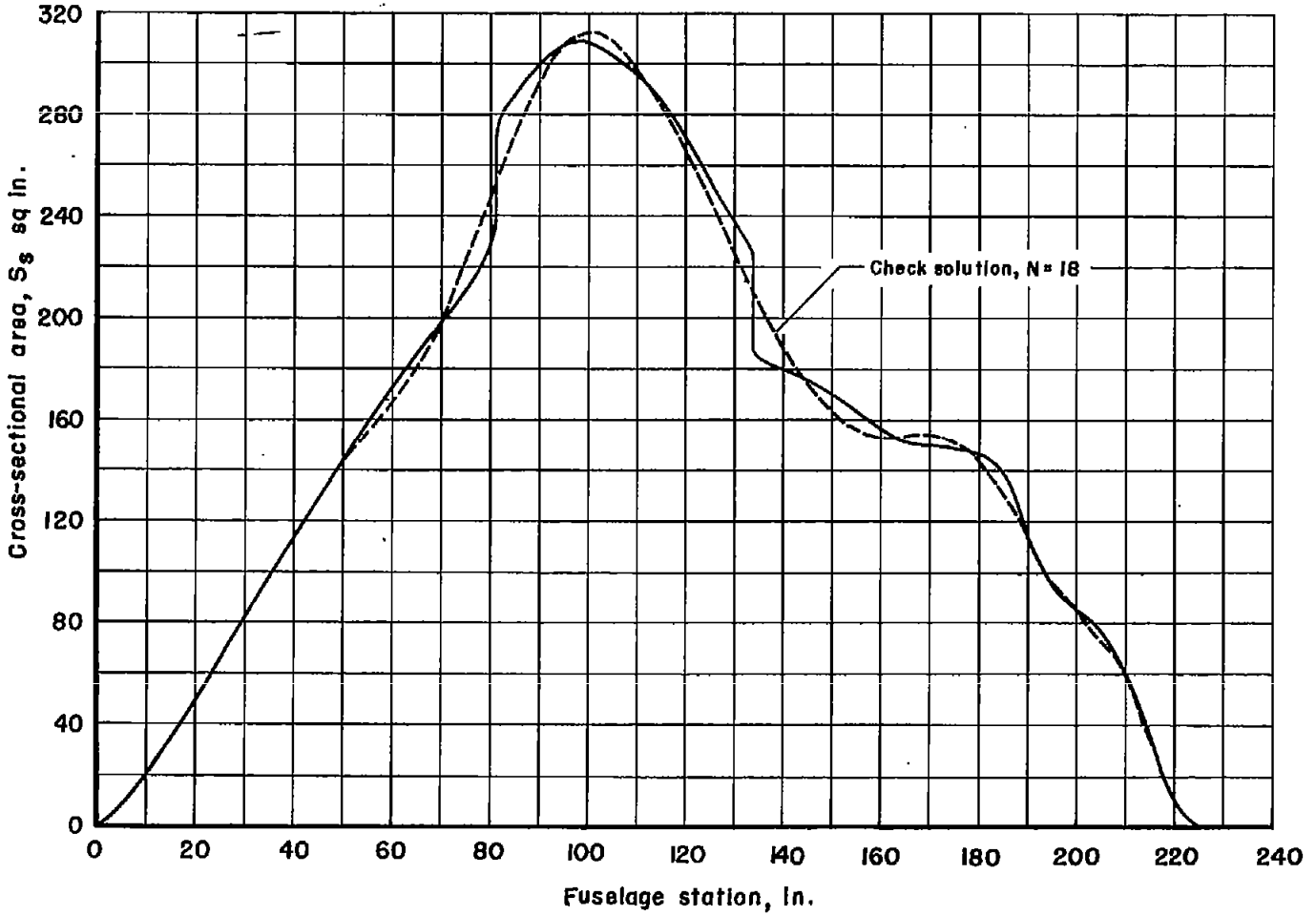

(b) Inadmissible solution for N = 18 which happens to give results comparable to experimental data.

Figure 14.- Concluded.